Available online at www.sciencedirect.com

ScienceDirect

Nuclear Data Sheets 145 (2017) 1–24

Nuclear Data Sheets

www.elsevier.com/locate/nds

Uncertainty-driven nuclear data evaluation including thermal (n,α) applied to ^{59}Ni

P. Helgesson*
Department of Physics and Astronomy, Uppsala University, Uppsala, Sweden and Nuclear Research and Consultancy Group NRG, Petten, The Netherlands

H. Sjöstrand
Department of Physics and Astronomy, Uppsala University, Uppsala, Sweden

D. Rochman
Paul Scherrer Institute PSI, Villigen, Switzerland

(Received 2 February 2017; revised received 6 July 2017; accepted 20 July 2017)

This paper presents a novel approach to the evaluation of nuclear data (ND), combining experimental data for thermal cross sections with resonance parameters and nuclear reaction modeling. The method involves sampling of various uncertain parameters, in particular uncertain components in experimental setups, and provides extensive covariance information, including consistent cross-channel correlations over the whole energy spectrum. The method is developed for, and applied to, ^{59}Ni, but may be used as a whole, or in part, for other nuclides.

^{59}Ni is particularly interesting since a substantial amount of ^{59}Ni is produced in thermal nuclear reactors by neutron capture in ^{58}Ni and since it has a non-threshold (n,α) cross section. Therefore, ^{59}Ni gives a very important contribution to the helium production in stainless steel in a thermal reactor. However, current evaluated ND libraries contain old information for ^{59}Ni, without any uncertainty information.

The work includes a study of thermal cross section experiments and a novel combination of this experimental information, giving the full multivariate distribution of the thermal cross sections. In particular, the thermal (n,α) cross section is found to be 12.7 ± .7 b. This is consistent with, but yet different from, current established values.

Further, the distribution of thermal cross sections is combined with reported resonance parameters, and with TENDL-2015 data, to provide full random ENDF files; all of this is done in a novel way, keeping uncertainties and correlations in mind. The random files are also condensed into one single ENDF file with covariance information, which is now part of a beta version of JEFF 3.3.

Finally, the random ENDF files have been processed and used in an MCNP model to study the helium production in stainless steel. The increase in the (n,α) rate due to ^{59}Ni compared to fresh stainless steel is found to be a factor of 5.2 at a certain time in the reactor vessel, with a relative uncertainty due to the ^{59}Ni data of 5.4%.

I. INTRODUCTION

A. Background

In many stainless steels, nickel makes up as much as 10% of the content, but ^{59}Ni does not occur in nature, as it is radioactive with a half-life of 76 000 years [1]. However, ^{58}Ni constitutes 68% of natural nickel, and this nuclide has a high thermal (n,γ) cross section, compared to the other major constituents of stainless steel, *i.e.*, iron and chromium [2]. As a result, a substantial fraction of the neutrons passing through stainless steel components in a thermal nuclear reactor will be captured in ^{58}Ni nuclides. In this way, ^{59}Ni is produced, and the ^{59}Ni content can become more than 4% of the initial ^{58}Ni content before it starts to decrease [3].

In turn, ^{59}Ni has a rare property which makes it important. Namely, it has extraordinarily high thermal (n,α) and (n,p) cross sections, *i.e.*, cross sections for neutron capture followed by the emission of an α-particle or a proton, respectively (12.3 ± 0.6 b and 2.0 ± 0.5 b, respectively [2]). This results in the production of helium and hydrogen gas in the steel even in thermal spectra,

*Corresponding author, electronic address: peter.helgesson@physics.uu.se

https://doi.org/10.1016/j.nds.2017.09.001

which leads to, *e.g.*, embrittlement of the material. The reactions also have high Q-values, such that substantial amounts of energy are released in the material, also leading to material damage. Thus, the *two-step* reactions ^{58}Ni(n,γ)^{59}Ni(n,α) and ^{58}Ni(n,γ)^{59}Ni(n,p) make ^{59}Ni important in thermal reactors [3].

In the major evaluated nuclear data libraries, ^{59}Ni does not have any covariance data. In ENDF/B-VII.1 [4], the ^{59}Ni file is copied from JEFF 3.2 [5], which in turn is copied from previous JEFF/JEF versions since JEF 2.2: an evaluation from ECN, Petten from 1990 [6]. The primary goals of this work are to provide a modern evaluation for ^{59}Ni, containing covariances, and to present novel ideas in nuclear data evaluation.

For the considered nuclide, there are two main sources of information based on experiments: several experiments on thermal cross sections, and a set of resonance parameters which is poorly documented (no raw data nor partial cross sections are available, to the knowledge of the authors, and the uncertainty information is limited). In this work, a methodology trying to make the best use of these two sources is developed, and which also takes knowledge from other nuclides into account, via physical models. At the heart of the methodology, there is random sampling of various uncertain parameters. The sampling of reaction model parameters and resonance parameters constitute similarities to Total Monte Carlo [7, 8], but experimental error components are also sampled, and the combination of the different sources of information is done in a novel way.

Some special care has to be taken because the most frequently used resonance parameter formats in the ENDF format [9] do not allow for thermal and resonance range (n,α) and (n,p) cross sections described by resonance parameters. The relatively new resonance format "`LRF=7`" allows for these channels, but it assumes more detailed knowledge of the available experiments.

Even if the methodology is developed to meet the situation of ^{59}Ni, it may very well be used for other nuclides with non-threshold reactions which are not allowed in the most common resonance parameter formats, such as (n,α) and (n,p). Further, many of the ideas in this work are even more general, and can be applied to any nuclide of interest.

B. Overview of the available experimental data

There are several experiments covering thermal cross sections, for (n,α), (n,p), (n,γ) and (n,tot); these experiments are discussed in Sec. II and described in more detail in Appendix A. On top of this, there are resonance parameters reported to EXFOR [10], primarily by Harvey (EXFOR entry 10680), including α and proton widths; these parameters are discussed more in Sec. III A. There are also total cross section experiments ranging from 6.6 meV to 0.21 MeV reported by Harvey and Raman. No satisfactory documentation for the above-mentioned resonance parameters nor for the total cross section measurements has been found, and the resonance parameters and the Harvey/Raman (n,tot) data is from the same period in time. The resonance parameters may partially be derived from this (n,tot) data and, therefore, the (n,tot) data is used for thermal cross sections and for the verification of the reconstructed cross sections only (see Sec. IV A).

C. Overview of the method and the paper's disposition

An overview of the work described in this paper is seen in Fig. 1. Note that data represented by all the three left-most boxes (thermal cross sections, resonance parameters and the nuclear reaction parameters of TALYS) are *sampled*, with the aim to yield a quantification of the uncertainty in the resulting ND. To begin with, the thermal cross sections are sampled based on uncertainties in the experimental setups, carefully considering correlations both within and across experiments. The random TALYS parameters used in TENDL 2015 [8] are used to give the random TALYS results, as in Total Monte Carlo. Resonance parameters are sampled partially based on the resonance parameters and uncertainties mentioned in Sec. I B. Also, positions and widths of resonances at negative energies (bound resonances) and in the unresolved range are sampled based on average level spacings and average resonance widths from TALYS.

For each sampled set of resonance parameters and thermal cross sections, the widths of the bound resonances are adjusted such that the thermal cross sections reconstructed from the resonance parameters match the thermal cross sections sampled from the experimental data. If the adjustment fails, the combination of the thermal cross sections and the rest of the data is considered unphysical, so the thermal cross sections and resonance parameters are sampled again. This rejection introduces correlations between all the different sets, since sets which are not compatible with each other will be discarded. Correlations between the different sets also arise from the use of random information from TALYS to sample resonance parameters and the inclusion of certain systematic errors from the thermal cross section experiments in the resonance parameters.

After the adjustment, we have a distribution of resonance parameters which is adjusted to the distribution of the thermal cross sections (based on the experimental data). Each set of random resonance parameters is combined with higher-energy cross sections, and data which are not cross sections (*e.g.*, angular distributions), from TALYS, for each set using the same random TALYS parameters as was used to obtain the corresponding resonance parameters. In other words, the distribution of resonance parameters is combined with a distribution of TALYS data, keeping track of correlations arising from the use of TALYS model parameters in both parts. This

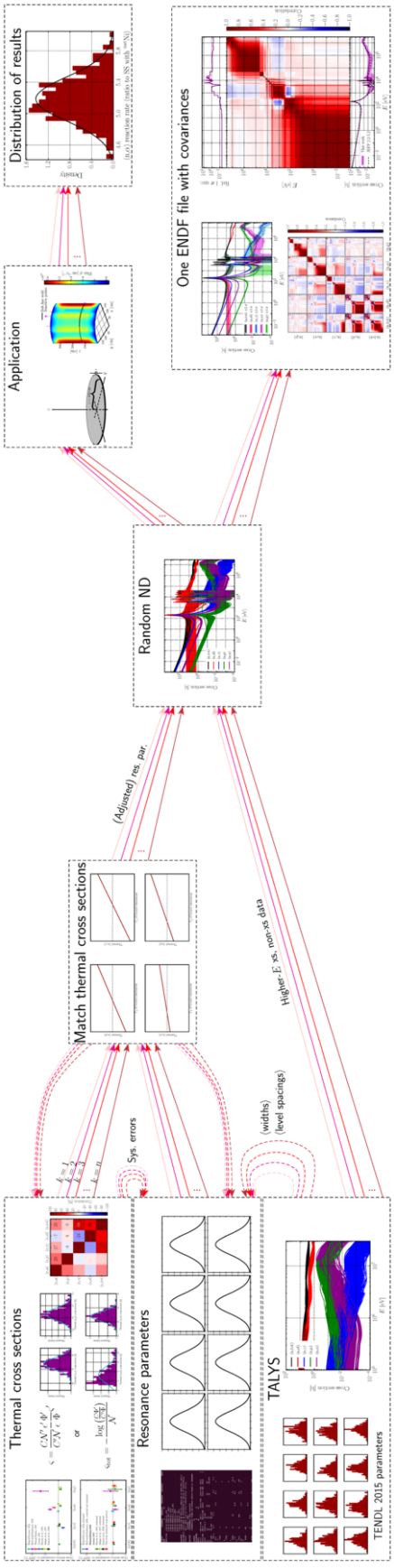

FIG. 1: (Color online) Overview of the work described in this paper. The multiple arrows between the different boxes represent the individual random sets of data.

results in a distribution of *complete* ND, which can be formatted into n different ENDF files. This can be used directly for Monte Carlo uncertainty propagation or to generate one single ENDF file with covariance information.

Sec. II discusses the experiments measuring the thermal cross sections, and how the uncertainties of these experiments are sampled. In Sec. III, the reader finds more details regarding the combination of these thermal cross sections with sampled resonance parameters and random TALYS results.

Integrity checks of the obtained distribution of the cross sections is performed using, *e.g.*, Harvey/Raman's total cross section data in Sec. IV. The generation of one single nuclear data file with covariance information is described in Sec. V. Finally, the random nuclear data files are used in a simple model of stainless steel in an LWR spectrum in Sec. VI.

Results are presented and discussed throughout the text, since this is believed to make the text easier to follow. Conclusions are found in Sec. VII.

II. EVALUTION OF EXPERIMENTAL THERMAL CROSS SECTIONS

There are several experiments which cover thermal cross sections for ^{59}Ni, ranging over (n,α), (n,p), (n,γ) and (n,tot). In analyzing the uncertainties of these experiments, an attempt is made to follow a working process which is as transparent and objective as possible, by treating the different experiments in a way which is as general as possible. This general treatment, which aims to estimate the uncertainty and correlations for the different *uncertainty components* in the experimental data, is described in Sec. II A.

The details of the analysis, experiment by experiment, are found in Appendix A. The resulting uncertainty components are summarized in Table III, and the differences between the original and evaluated experimental information are visualized in Fig. 2.

In Sec. II B it is described how the information from the experiments is merged together by sampling the experimental uncertainty components found in Sec. II A. This is analogous to how the *nuclear model parameters* are sampled in Total Monte Carlo [8]. The sampling of systematic uncertainty components is similar to the sampling of systematic errors in Ref. [11]. However, the aim of the sampling in Ref. [11] is to compute the likelihood when comparing model parameters to experiments, while the sampling in this work aims to *directly* yield the distribution of experimental data.

A. Uncertainty components

Somewhat simplified, a typical reaction cross section measurement is carried out by letting a neutron beam

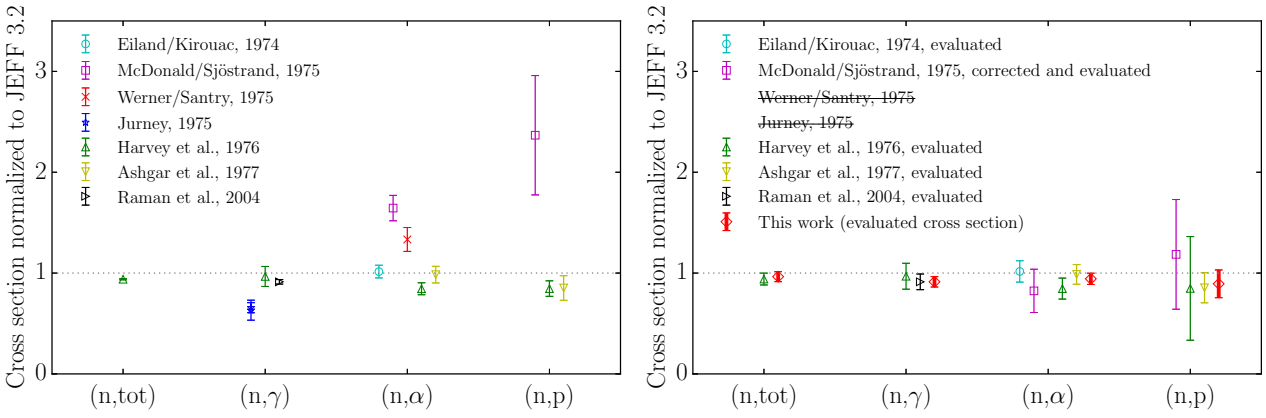

(a) As reported.

(b) Evaluated, corrected, renormalized and compared to the evaluated thermal cross sections resulting from Sec. II (including physical constraints).

FIG. 2: (Color online) Experimental thermal cross sections, normalized to JEFF 2.2-3.2 to enable presentation in one graph.

TABLE I: Default relative uncertainties for the constituents of Eq. (1), (3) or (5) as well as the background subtraction, used if other information is not found. The same values are used for the corresponding monitor values.

	Rel. std. dev. (%)
Background	1
Impurities (n,tot)	2
ϵ'/ϵ	2
ϵ	5
$\mathcal{N}$	5
N	3
d	4
ϕ'/ϕ	2

with flux ϕ hit a target containing $\mathcal{N}$ nuclei of interest during time t and detecting the number of counts C (of a certain type) in a detector with efficiency ϵ, and the cross section ς is obtained from[1]

$$\varsigma = \frac{C}{\epsilon \mathcal{N} \phi t}, \tag{1}$$

using a thin sample approximation; see, *e.g.*, Refs. [12, 13]. It is assumed that the typically unavoidable background is already subtracted from C.

The flux is implicitly or explicitly estimated using a monitor cross section ς', which is assumed to be known, by rearranging Eq. (1) to

$$\phi' = \frac{C'}{\epsilon' \mathcal{N}' \varsigma' t'}, \tag{2}$$

where the prime ($'$) denotes that all quantities now relate to the monitor cross section.

[1] Note that cross sections are denoted "ς" in this work, to avoid confusion with the standard deviation σ.

Multiplying Eq. (1) with ϕ'/ϕ' and inserting this expression for ϕ' (once), one obtains

$$\varsigma = \frac{C \mathcal{N}' t'}{C' \mathcal{N} t} \frac{\epsilon'}{\epsilon} \frac{\phi'}{\phi} \varsigma'. \tag{3}$$

Normally, $\phi'/\phi \approx 1$ is expected, but there can be an instability in the flux, and the exact same setup may be difficult to reproduce, such that ϕ'/ϕ has an uncertainty.

For measurements of the total cross section $\varsigma_{(\mathrm{n,tot})}$, transmission experiments are used. The transmission T is determined by [14]

$$T = \frac{C \phi' t'}{C' \phi t} = e^{-N d \varsigma_{(\mathrm{n,tot})}}, \tag{4}$$

where the primed quantities now refer to a measurement *without* a target, and where N is the nuclide density and d is the sample thickness. Thus, the cross section is obtained from

$$\varsigma_{\mathrm{tot}} = -\frac{\ln(T)}{Nd} = -\frac{\ln\left(\frac{C\phi' t'}{C' \phi t}\right)}{Nd}. \tag{5}$$

No reference cross section is needed and the detector efficiencies cancel out since only neutrons with the same energies are detected. However, the transmission is directly affected by the total cross section of other present nuclides in the sample. We account for this with an additional 2% default uncertainty in the background correction included in C. The choice of 2% can be discussed; however, it should have a limited impact on the results since it is applied to only one thermal experimental point.

For reaction cross sections, Eq. (1) is used if an uncertainty estimate for the flux is quoted, and otherwise Eq. (3) applies. In any case, Eq.(5) is used for (n,tot). From studying the articles (or EXFOR entries if the articles are

not found), we try to deduce which quantities were included in the original uncertainty analysis. Uncertainties due to contributions in Eq. (1), (3), or (5) which are not accounted for are added according to the values quoted in Table I. These values are based on the uncertainty estimates found in the (other) considered publications. For example, uncertainties between 3% [15, 16] and 6% [15] are quoted for the target thicknesses d and d', and values of about 1% [17] and 2% [15] are quoted for the densities N and N'. The default values 4% and 3% for d and N combine to 5% for $\mathcal{N}$, assuming that they are independent and dominate the uncertainty in $\mathcal{N}$. For the detector efficiency, 2.5% is quoted in Ref. [13]. It refers only to a statistical calibration uncertainty, and we believe there are other uncertainties, too. A flux uncertainty of 3.6% is quoted in Ref. [13], and the uncertainties of the ratios ϕ'/ϕ and ϵ'/ϵ are assumed a little less because of the desired cancellation of parts of the errors. Typically, we choose the default values to be a little larger than the average quoted values, to be on the conservative side. It is difficult to avoid a certain amount of subjectivity, and the chosen numbers may be debated. However, the general assumptions are clearly stated in Table I, and the detailed breakdown into individual uncertainty components enables a motivated correlation structure.

On top of the explicit constituents of the equations, an uncertainty due to the correction for background and impurities is also included in Table I, while the exposure times t and t' are considered to be exactly known; they are typically on the order of hours or days, so they could easily be determined with high relative precision. The uncertainty in $\mathcal{N}$ is considered to be dominated by the thickness d and the nuclide density N.

Typically, the procedure increases the uncertainty compared to what is quoted in the original paper. If an estimate for the flux is quoted (in which case Eq. (1) is used), this uncertainty is scaled to obtain the same relative increase as the rest of the uncertainties. See Appendix A 1 for an example (the only experiment considered here which quotes a flux uncertainty).

Finally, the reference cross sections are used for renormalization and to add correlated uncertainty components according to the current neutron cross section standards [18]. Reference cross sections other than the ^{6}Li(n,t) cross section have greater relative uncertainty than that of ^{6}Li(n,t). To simplify, their relative errors are assumed to consist of the relative error in ^{6}Li(n,t), and another component independent of ^{6}Li(n,t). That is, full correlation is assumed between the reference cross sections for uncertainties up to the relative uncertainty of ^{6}Li(n,t), which is 0.13%. The rest of the uncertainty is considered uncorrelated to the other reference cross sections.

B. Merging the information on thermal cross sections

The uncertainty information deduced according to the above is summarized in Table II. Using this information and Eqs. (1) and (3), the error components are sampled (see Sec. II B 2). This yields a sample from the distribution of the thermal cross sections, which is used in the generation of random ND files in Sec. III A.

1. *Renormalizing relative uncertainties*

The correlations between the different uncertainties are carefully taken into account in this work. As a first step, however, the weighted mean values ignoring the correlations of each cross section are obtained, using the inverse of the summed variance as weight. This calculation is done for one single purpose, namely, to renormalize the relative uncertainties such that they are relative to this weighted mean. For example, the weighted mean value of the (n,γ) cross section measurements is 74.76 b. Then, the relative uncertainties of the (n,γ) cross section from Appendix A 7 (last line of Table II) are multiplied by the factor 74.76/73.7, such that, *e.g.*, the "Combined" uncertainty becomes 4.49% instead of 4.43%. This is done for two reasons:

1. The relative uncertainties should be relative to the expected value, and the weighted mean from different measurements is a better estimate of this

2. In Ref. [19], it was seen that a similar treatment could help to avoid the problem of the so-called Peelle's pertinent puzzle [20].

Another reason for Peelle's pertinent puzzle which has been pointed out is linearization of non-linear functions [21]. This is also avoided in this work, which becomes clearer in the following sections.

For completeness, the weighted averages are found in part *i* of Table III. Their uncertainties are also given, for later comparison.

2. *Sampling error components to estimate cross sections*

After the renormalization of the uncertainties, the relative error components listed in Table II are sampled, with full correlations according to the alphabetical superscripts. The "Combined" uncertainty in the Eiland/Kirouac experiment is sampled from a t-distribution with 5 degrees of freedom because of how the estimate was obtained (see Appendix A 1), and the others are sampled from a distribution which is based on the normal distribution, but transformed such that negative values are avoided, using a superposition of a normal distribution and an exponential distribution in each dimension. The reference cross sections are used for renormalization with

TABLE II: Relative uncertainties (1 std. dev., in %) for different constituents of Eq. (1), Eq. (3) or Eq. (5) for the thermal cross section measurements summarized in Appendix A. Latin alphabetical superscripts indicate (assumed) full correlation between uncertainties with the same superscript. Similarly, Greek alphabetical superscripts stand for full correlation for half the variance. Asterisks (∗) indicate that the uncertainty is included in the "Combined" row (if a number is given, too, *the rest* of the uncertainty is included in "Combined"). †: should be sampled from t-distribution with 5 degrees of freedom. ††: Assumed reference value based on experiments near in time. ♡: Full correlation assumed up to the relative uncertainty of ^{6}Li(n,t), with the rest uncorrelated. ♢: Measured relative to ^{58}Ni (n,γ), in turn relative to ^{1}H(n, γ).

Appendix	A.1	A.3		A.5				A.6				A.7
Reaction	(n,α_0)	(n,α_0)	(n,p$_0$)	(n,tot)	(n,γ)	(n,α_0)	(n,p$_0$)	(n,α_0)	(n,α_1)	(n,p$_0$)	(n,p$_1$)	(n,γ)
Est. [b]	13.7	11.1	2.0	92.28	78	11.4	1.43	13.1	0.188	1.34	0.10	73.7
Combined	6.54†	-	-	-	-	-	-	7.38	7.51	12.8	100	4.43
C	∗	1.35	1.35	0.631	10.3	7.02	9.09	∗	∗	∗	∗	∗
Backg.	∗	1	50	$\sqrt{1^2+2^2}$	1	1	50	1	1	1	∗	1
ϵ	3.20*	-	-	-	-	-	-	-	-	-	-	-
$\mathcal{N}$	5	-	-	5^{e}	5^{e}	5^{e}	5^{e}	-	-	-	-	-
N	-	2^{a}	2^{a}	-	-	-	-	2^{a}	2^{a}	2^{a}	∗	∗
d	-	3^{b}	3^{b}	-	-	-	-	3^{b}	3^{b}	3^{b}	∗	4
ϕ	5.85	-	-	-	-	-	-	-	-	-	-	-
ϵ'/ϵ	-	2	2	-	2	2	2	2	2	2	∗	2
$\mathcal{N}'$	-	-	-	-	5^{f}	5^{f}	5^{f}	-	-	-	-	-
N'	-	20^{c}	20^{c}	-	-	-	-	3^{g}	3^{g}	3^{g}	∗	∗
d'	-	6^{d}	6^{d}	-	-	-	-	4^{h}	4^{h}	4^{h}	∗	4
ϕ'/ϕ	-	2$^{\alpha}$	2$^{\alpha}$	2**	2$^{\beta}$	2$^{\beta}$	2$^{\beta}$	∗	∗	∗	∗	2
ς'	0.14^{i} ♡	0.13^{i}	0.13^{i}	-	0.13^{i}	0.13^{i}	0.13^{i}	0.13^{i}	0.13^{i}	0.13^{i}	0.13^{i}	0.21^{i} ♡
Ref. reaction	^{197}Au(n,γ)	^{6}Li(n,t)	^{6}Li(n,t)	^{6}Li(n,t)	^{6}Li(n,t)	^{6}Li(n,t)	^{6}Li(n,t)	^{6}Li(n,t)	^{6}Li(n,t)	^{6}Li(n,t)	^{6}Li(n,t)	^{1}H(n,γ)♢
Ref. value	98.8††	940	940	940, 941††	940, 941††	940, 941††	940, 941††	941	941	941	941	0.3326

current values (^{6}Li(n,t) and ^{197}Au(n,γ) from Ref. [18] and ^{1}H(n,γ) from Ref. [2]), and corresponding error components are also sampled according to Table II.

In this way, all experiments are "simulated" simultaneously n_0+n times. The first n_0 simulations are performed only to give estimates for the covariance for the different experimental points for each reaction. These covariance estimates are used for the last n simulations, where generalized least squares [22] is used for each reaction to obtain the estimate for that cross section for *that particular simulation*. In this work, $n_0 > 10^5$, while n varies for the different steps below (there is a certain progression in the estimates).

For each simulation, the partial (n,α) and (n,p) cross sections are summed up, and the elastic cross section is obtained as

$$\varsigma_{(\mathrm{n,el})}^{(k')} = \varsigma_{(\mathrm{n,tot})}^{(k')} - \varsigma_{(\mathrm{n},\gamma)}^{(k')} - \varsigma_{(\mathrm{n},\alpha)}^{(k')} - \varsigma_{(\mathrm{n,p})}^{(k')}, \tag{6}$$

where $k' \in \{1, 2, ..., n_0 + n\}$ denotes simulation number k' and the different cross sections ς are labeled by their respective reactions.

Using $n = 40\,000$, the mean values and standard deviations in part *ii* of Table III are obtained, and the correlation matrix is shown in Fig. 3(a). The values differ indeed from those obtained using the simple weighted mean, so the correlations and/or the nonlinearities certainly had an impact. Both the mean values and the standard deviations are slightly greater than for the weighted mean values, except for (n,el). The generally greater mean values and standard deviations can be caused by the sampling of error components in the denominators of Eqs. (1), (3), or (5); this can be seen to cause greater expected values and variances than when adding relative uncertainties in quadrature. The smaller standard deviation for (n,el) can be explained by the positive correlations between (n,tot) and the other cross sections (which arise from common systematic uncertainties). Except for (n,el), all cross sections are positively correlated as one could expect because of the common systematic uncertainties. The (n,el) cross section is positively correlated to (n,tot) and negatively correlated to the other cross sections as a consequence of Eq. (6); however, the correlations to (n,α) and (n,p) are weak. This can be explained by that their absolute uncertainties are smaller than for (n,tot) and that they are positively correlated to (n,tot).

Note that the mean, standard deviation, and the correlations only reflect limited aspects of the (joint) distribution of the cross sections, but that a random sample from the full distribution is used in the production of the random ND files in Sec. III.

3. *Including physical constraints for better estimates*

On top of the experimental information, we *also* know, *e.g.*, that the cross sections are non-negative. In particular, we know that this holds for the (n,el) cross section, while there is a risk that a simulation according to the above will result in negative values, if the (n,tot) cross section happens to be less than the sum of the others. Bayes' theorem gives that one can simply reject physically impossible results from the sample, and redraw it

TABLE III: Estimated expected values $\langle\varsigma\rangle$ and standard deviations $\sigma(\varsigma)$ in barns for the thermal cross sections obtained at the different stages of the evaluation of the thermal cross sections, and also the values from Mughabghab [2] and the evaluation contained in JEFF 2.2-3.2 [5] (which is copied into ENDF/B-VII.1 [4]). The quoted uncertainties in the expected values are one standard deviation of the mean, while the uncertainties of the standard deviations are determined using the method described in Ref. [23]. The progression in this work starts with *i* moving through *iv*.

			(n,α)		(n,p)		(n,γ)		(n,el)		(n,tot)	
			$\langle\varsigma\rangle$	$\sigma(\varsigma)$	$\langle\varsigma\rangle$	$\sigma(\varsigma)$	$\langle\varsigma\rangle$	$\sigma(\varsigma)$	$\langle\varsigma\rangle$	$\sigma(\varsigma)$	$\langle\varsigma\rangle$	$\sigma(\varsigma)$
This work	*i*	W. mean	12.6	.715	1.46	.207	74.8	4.98	3.42	7.39	92.3	5.67
	ii	Sim.	12.833(4)	0.728(3)	1.479(1)	0.2066(8)	74.92(3)	5.02(2)	3.13(4)	7.06(2)	92.36(3)	5.85(2)
	iii	Sim. + el. > 0	12.820(4)	0.729(3)	1.477(1)	0.2066(8)	73.28(2)	4.42(2)	6.87(2)	4.87(2)	94.44(3)	5.23(2)
	iv	Sim. + "physics"	12.73(4)	.71(3)	1.51(1)	.209(9)	73.7(2)	3.8(2)	6.8(2)	3.5(2)	94.8(3)	4.7(2)
	v	Mughabghab	12.3	0.6	2.0	0.5	77.7	4.1	-	-	-	-
	vi	JEFF 2.2-3.2	13.5	-	1.69	-	80.7	-	2.33	-	98.3	-

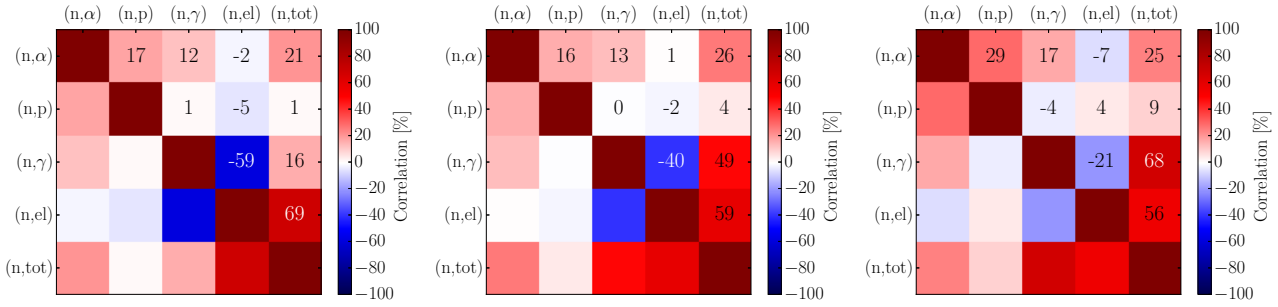

(a) Without physical constraints. $\Delta_s \lesssim 0.5$ %. Corresponds to part *ii* in Table III.

(b) Positive (n,el). $\Delta_s \lesssim 0.5$ %. Corresponds to part *iii* in Table III.

(c) Additional physical constraints, see Sec. III B. $\Delta_s \approx 5$ %. Corresponds to part *iv* in Table III.

FIG. 3: (Color online) The correlations (%) between the different thermal cross sections obtained from the simulation of experimental error components. The sampling uncertainties (one standard deviation) Δ_s are estimated analogously to the uncertainty of uncertainty in Ref. [23].

from the original distribution (perform a new simulation), as is shown in Appendix B.

In this way, the simulations are redone using the condition that the elastic cross section must be non-negative. Again using $n = 40\,000$ accepted simulations, this gives the mean values and standard deviations of part *iii* of Table III, and the correlations illustrated in Fig. 3(b). The distribution has clearly changed. The distribution for (n,el) is (not surprisingly) pushed towards greater values; the new mean value is more than twice as large as before, and the uncertainty decreases. However, the relative uncertainty is still very large. As a natural consequence of the increasing elastic cross section, (n,tot) also increases. Otherwise, the most significant difference is a decrease of the (n,γ) cross section, probably because it is the main constituent of the (n,tot) cross section; a small (n,γ) will reduce the risk of a negative (n,el). The correlations are also affected by the constraint. In particular, the correlation between (n,tot) and (n,γ) increases from 16% to 49%, since the restriction on (n,el) only allows (n,γ) to be large if (n,tot) is large, too.

When the resonance parameters are adjusted to match the thermal cross sections (described in Sec. III B), it turns out that the adjustment procedure fails to converge in many cases, see Sec. III B. If the adjustment does not converge, we consider that the combination of the simulated values of ς and the rest of the ND is "unphysical", and we redo the simulation of the thermal cross sections and redraw the resonance parameters, analogously to when redrawing results with negative cross sections.

This procedure results in the mean values and standard deviations in part *iv* of Table III, and the correlation matrix illustrated in Fig. 3(c). This affects the distribution of the cross sections further. For example, the uncertainties of (n,el) and (n,tot), and the (n,α) cross section decreases somewhat. However, since this is time-consuming, the procedure is only followed for the random ND files that actually are produced, and the numbers here are based on $n = 300$ accepted simulations, so the statistics are poorer, compared to the previous steps.

For all results presented here, the effect of the finite sample size n is estimated and reported as "sampling uncertainty". For standard deviations and correlations, this is done by repeatedly dividing the sample into subsets as described in Ref. [23]. If one is interested in mean values and standard deviations, it is often enough with a sample size of 300; this yields an uncertainty of the mean which is a 17th ($17 \approx \sqrt{300}$) of the uncertainty, and an uncertainty of the standard deviation of approximately 4%, relative to the uncertainty. The latter number assumes

a normal distribution, but it agrees well with the results obtained using the method in Ref. [23] (which does not assume a normal distribution). These observations also hold for propagated results. If computations are cheap, there is no reason not to improve the accuracy by using a larger sample size such as $n = 40\,000$.

Finally, we may note that the mean values and standard deviations are different from, but still compatible with, the corresponding values from The Atlas of Neutron Resonances [2] and what is found in JEFF 2.2-3.2 and ENDF/B-VII.1 (which lack uncertainties), see Table III.[2] For the possibly most important cross section, (n,α), the value obtained in this work is in between the corresponding values in Ref. [2] and JEFF. The quoted uncertainties in this work are similar to those in Ref. [2] for (n,α) and (n,γ), but smaller for (n,p). Note that in this work, the full joint distribution of the different cross sections is estimated.

III. COMBINING THERMAL CROSS SECTIONS WITH RESONANCE PARAMETERS AND TALYS RESULTS

A. Resonance parameters

Except for the measurements on thermal cross sections summarized in Appendix A, EXFOR contains experimental cross section data for the total cross section for higher energies. This data comes from the same series of measurements as described in Appendix A 5 (for which we did not find much documentation), and from Raman, 1975. Both sets of data are from ORNL, and Harvey is a coauthor of the Raman data set; it also has the same problem with the documentation. In the same EXFOR entry as the Harvey data in Appendix A 5, parameters for resolved resonances are also reported, referring to "Harvey, Private communication, 1980". The resonance parameters are resonance energies E_λ, neutron, γ, α and proton widths (Γ_n, Γ_γ, Γ_α and Γ_p) and quantum numbers ℓ and J, for each level λ. These parameters are tabulated in Table IV, where they are also compared to the parameters finally obtained in this work. For one energy (203.4 eV), there are also some resonance parameters reported by Kirouac, 1975, but this does not include α and p-widths. Since the different widths should be determined simultaneously, the Kirouac parameters are ignored.

Because it is likely that some of the resonance parameter data has its origin in the reported cross section data, one should not carelessly make use of both. Therefore, we use only the resonance parameters of Harvey, and leave the (n,tot) cross section measurements for verification of the results.

In this work, the resonance parameters can be divided into three categories: resolved resonance parameters, unresolved resonance parameters and parameters for bound resonances. The treatment of these three categories is found in Secs. III A 1, III A 2, and III A 3, respectively. For some of the resonances, Harvey does not give the complete set of parameters. This is treated by sampling the missing information, building upon the sampling of completely unmeasured resonances in Secs. III A 2 and III A 3. The technical details are found in Appendix C.

1. *Sampling completely reported resonance parameters*

Harvey's resonance parameters are sampled using normal distributions with expected values and standard deviations from the central values and uncertainties provided in the EXFOR entry. Parameters given as an upper limit are assumed to be exponentially distributed (which results in a 100% uncertainty) with 1/3 of the upper limit as expected value. This choice is made to give only a small probability (5%) to exceed the upper limit and to get an increasing probability density close to zero. The choice can be discussed, but it will have an impact only on quantities which are very uncertain and, typically, small in magnitude, therefore having a limited impact on results. We believe it is more reasonable to assume an exponential distribution than, say, a uniform distribution since an upper limit is likely to have its origin in an undetected result which are likely to be caused by values close to zero.

On top of sampling from the provided uncertainties, we *approximate* the systematic errors sampled for Harvey's thermal cross section data for the reaction cross sections. For the fully correlated uncertainty components for (n,γ), (n,α) and (n,p) in the Harvey experiment in Table III, the approximation is done by adding the same relative errors $\Delta_\gamma, \Delta_\alpha$ and Δ_p, respectively, to each of $\Gamma_{\gamma\lambda}, \Gamma_{\alpha\lambda}$ and $\Gamma_{\mathrm{p}\lambda}$ for all resonance levels λ. It is assumed that

$$\varsigma_{(\mathrm{n,r})}(E) = h_\mathrm{r}(E) \sum_\lambda \Gamma_{\mathrm{r}\lambda}, \tag{7}$$

for some function $h_\mathrm{r}(E)$ which does not depend on any $\Gamma_{\mathrm{r}\lambda}$, and where $\mathrm{r} \in \{\gamma, \alpha, \mathrm{p}\}$. This equation approximates the corresponding Multi-Level Breit-Wigner (MLBW) formulas if $|E - E_\lambda| \gg \Gamma_\lambda$ (where Γ_λ is the total width) for all λ [9], *i.e.*, everywhere not too close to a resonance. When adding the relative errors above, the resulting cross sections become

$$\varsigma_{(\mathrm{n,r})}(E) + \Delta\varsigma_{(\mathrm{n,r})}(E) = h_\mathrm{r}(E) \sum_\lambda \Gamma_{\mathrm{r}\lambda} \left(1 + \Delta_\mathrm{r}\right), \tag{8}$$

where $\Delta\varsigma_{(\mathrm{n,r})}(E)$ is the resulting error in $\varsigma_{(\mathrm{n,r})}(E)$. This yields that the resulting relative errors in the cross sec-

[2] For the (n,el) cross section, the JEFF 2.2-3.2 value is not within *one* standard deviation, but rather 1.3 standard deviations. Assuming normal distributions, this corresponds to a p-value of 20%, and we consider this consistent.

Harvey's quoted resonance parameters (from EXFOR entry 10680) with quoted uncertainties, as well as the mean values and uncertainties obtained in this work, discussed in Sec. III F. The quoted sampling uncertainties in the expected values are one standard deviation of the mean, while the sampling uncertainties of the standard deviations are determined using the method described in Ref. [23]. The values of this work which deviate more than 3 standard deviations in sampling uncertainty from Harvey's quoted values are highlighted in boldface. For the cases with sampled ℓ and J (when not provided by Harvey), the observed relative frequencies are found in Table VIII. Asterisks (*) indicate that an upper limit was given in Harvey's data; the quoted value is 1/3 of this limit, and a 100% uncertainty is used. The three latter quantities are not stored in the ENDF files produced later, and only computed for this work when given in Harvey's data, for verification purposes. There are also resonances noted by Harvey at (1333 ± 1) eV and (1742 ± 2) eV , both with $(\ell, J) = (0, 2)$, and small values given for $\Gamma_n\Gamma_p/\Gamma_{tot}$. When studying (n,tot) data (see Sec. IV A), these resonances cannot be clearly distinguished, so they are *only* used in the determination of (ℓ, J) for other resonances.

	E_λ	σ	$\langle\Gamma_n\rangle$	σ	$\langle\Gamma_\gamma\rangle$	σ	$\langle\Gamma_\alpha\rangle$	σ	$\langle\Gamma_p\rangle$	σ	$\langle\ell\rangle$	σ	$\langle J\rangle$	σ	$\langle\Gamma_{tot}\rangle$	σ	$\left\langle\frac{\Gamma_\alpha\Gamma_n}{\Gamma_{tot}}\right\rangle$	σ	$\left\langle\frac{\Gamma_p\Gamma_n}{\Gamma_{tot}}\right\rangle$	σ
Harvey	203.40	.20	9.60	.20	3.10	.30	.430	.030	.0550	.0050	.0	.0	1.0	.0	–	–	–	–	–	–
This work	203.40(1)	.195(8)	**9.54(1)**	.203(9)	**2.63(1)**	**.21(1)**	**.415(2)**	**.040(2)**	**.0331(9)**	**.0148(5)**	0	.0	1	.0	–	–	–	–	–	–
Harvey	3203.0	1.0	11.2	1.5	.80	.20	.00020*	.00020	.124	.080	1.0	.0	2.0	.0	–	–	–	–	–	–
This work	3202.92(6)	.97(4)	11.15(9)	1.52(6)	.79(1)	.209(8)	.00019(1)	.00019(2)	.123(6)	.099(7)	1	.0	2	.0	–	–	–	–	–	–
Harvey	4211.0	3.0	183	12	3.7	1.0	.1400	.0040	.2900	.0070	.0	.0	1.0	.0	–	–	–	–	–	–
This work	4210.9(2)	3.0(1)	182.7(7)	12.1(5)	**3.51(6)**	.98(4)	**.1353(6)**	**.0105(5)**	.273(8)	**.133(8)**	0	.0	1	.0	–	–	–	–	–	–
Harvey	6230	20	–	–	.20*	.20	–	–	–	–	–	–	–	–	–	–	–	–	–	–
This work	6231(1)	19.0(8)	70(8)	140(18)	.20(1)	.20(1)	.14(3)	.48(9)	.19(3)	.48(7)	.44(3)	.498(3)	1.68(3)	.55(3)	–	–	–	–	–	–
Harvey	6276	10	265	20	.90	.40	.0016	.0011	.00310	.00060	1.0	.0	2.0	.0	–	–	–	–	–	–
This work	6276.2(6)	9.6(4)	264(1)	19.5(8)	.90(2)	.42(1)	.00154(7)	.0012(1)	.00291(9)	**.00163(6)**	1	.0	2	.0	–	–	–	–	–	–
Harvey	6360	20	–	–	.20*	.20	–	–	–	–	–	–	–	–	–	–	–	–	–	–
This work	6360(1)	20.0(8)	63(7)	122(11)	.20(1)	.19(1)	.21(4)	.7(2)	.19(3)	.5(1)	.57(3)	.496(4)	1.65(3)	.54(2)	–	–	–	–	–	–
Harvey	9103	20	64	27	1.10	.23	.230	.020	.051	.013	1.0	.0	1.0	.0	–	–	–	–	–	–
This work	9102(1)	20.7(8)	61(2)	28(1)	1.08(1)	.24(1)	**.220(2)**	**.027(1)**	.049(2)	**.029(1)**	1	.0	1	.0	–	–	–	–	–	–
Harvey	9227	20	–	–	1.7*	1.7	–	–	–	–	–	–	–	–	30	15	–	–	–	–
This work	9229(1)	20.5(9)	17.6(8)	14.2(6)	1.7(1)	1.7(1)	5.4(5)	8.6(7)	5.4(5)	8.8(8)	.71(3)	.45(1)	1.85(3)	.45(4)	30.1(8)	13.8(5)	–	–	–	–
Harvey	9850	30	–	–	.40*	.40	–	–	–	–	–	–	–	–	6.6	6.6	–	–	–	–
This work	9850(2)	30(1)	4.6(3)	5.4(5)	.37(2)	.38(3)	.7(1)	1.7(2)	1.1(2)	2.7(4)	.64(3)	.480(8)	1.83(2)	.43(4)	6.7(4)	6.5(5)	–	–	–	–
Harvey	11100	30	–	–	2.0*	2.0	.010*	.010	.390	.040	–	–	–	–	40	20	–	–	–	–
This work	11104(2)	28(1)	38(1)	19.7(8)	2.0(1)	1.8(1)	.0089(5)	.0090(7)	**.376(2)**	.043(2)	.54(3)	.499(3)	1.987(7)	.11(3)	41(1)	19.7(8)	–	–	–	–
Harvey	11530	30	–	–	1.4*	1.4	.010*	.010	.240	.030	–	–	–	–	60	30	–	–	–	–
This work	11530(2)	30(1)	56(2)	30(1)	1.36(8)	1.4(1)	.0103(6)	.0107(7)	**.233(2)**	.032(1)	.51(3)	.5008(4)	1.94(1)	.25(3)	58(2)	30(1)	–	–	–	–
Harvey	14400	70	–	–	–	–	–	–	–	–	–	–	–	–	–	–	–	–	.080	.020
This work	14399(4)	68(3)	125(14)	247(24)	1.62(7)	1.1(1)	.36(5)	.8(1)	.6(2)	3(1)	.50(3)	.5008(2)	1.55(3)	.56(2)	–	–	–	–	.080(1)	.0197(8)
Harvey	17200	80	–	–	–	–	–	–	–	–	–	–	–	–	–	–	.11	.020	.060	.020
This work	17195(5)	78(3)	120(16)	281(42)	1.59(7)	1.1(1)	.7(1)	2.5(6)	.4(1)	1.9(6)	.55(3)	.498(3)	1.64(3)	.53(2)	–	–	**.106(1)**	.0185(8)	.057(1)	.0210(8)

tions are

$$\frac{\Delta\varsigma_{(\mathrm{n,r})}(E)}{\varsigma_{(\mathrm{n,r})}(E)} = 1 + \Delta_{\mathrm{r}}. \tag{9}$$

Thus, the fully correlated experimental errors in the reaction cross sections are approximated by adding the same relative errors to the corresponding widths. Note that the relative errors obtained for Harvey's thermal cross section experiment are used. Further, the uncorrelated systematic uncertainty components are added as relative uncorrelated uncertainties on the corresponding resonance parameters using Eq. (9) as motivation, even if this will give correlations between neighboring points.

For the elastic cross section it is not as easy to find a simplified analytic expression, and no attempt to approximate the systematic (n,tot) uncertainties is done. However, the above procedure will infer increased uncertainties on the (n,tot) cross section as well.

2. *URR parameters and sampling of resonances in the unresolved range*

For energies between 38.9 keV and 336 keV, each random set of nuclear data is provided with URR parameters from TALYS 1.8 [24] for the same set of random parameters as used in TENDL-2015 [8], *i.e.*, the URR parameters will vary between the random files, consistently correlated to the other information from TALYS. For energies between $E_{\mathrm{URR},0} = 17.2\,\mathrm{keV}$ and $E_{\mathrm{URR},1} = 38.9\,\mathrm{keV}$, resonances are *sampled* based on the same set of URR parameters, similarly to how the URR parameters are used in, e.g., the NJOY module PURR [25] to produce probability tables. This is also similar to the sampling of resonance parameters in Refs. [26, 27], but with a few differences. Only one random ladder of resonance energies is sampled in Refs. [26, 27], while, in this work, one random set of resonances (including their positions) is sampled for *each* random set of ND, and each time using URR parameters obtained from the corresponding random TALYS parameters. However, the distribution of the resonance energies is somewhat simplified in this work (Wigner distribution), compared to Refs. [26, 27].

In this work, resonance ladders are sampled for all combinations of orbital angular momenta ℓ and resonance spins J for $\ell \in \{0, 1, 2\}$. For each such (ℓ, J), the ladder starts from the highest energy resonance. For each step in the ladder, the energy increment to the next resonance is sampled using the Wigner distribution (a semicircle) with expected value and radius equal to the average level spacing given by TALYS at the energy[3] E_λ of the starting step (the URR parameters vary slowly with energy), $D^{\ell,J}(E_\lambda)$. The widths are sampled using the χ^2-distribution with expected values according to the URR parameters and $\nu_{\mathrm{n}} = 2, \nu_\gamma = 10, \nu_\alpha = 1$ and $\nu_{\mathrm{p}} = 1$ degrees of freedom (DOF) for $\Gamma_{\mathrm{n}}^{\ell,J}, \Gamma_\gamma^{\ell,J}, \Gamma_\alpha^{\ell,J}$ and $\Gamma_{\mathrm{p}}^{\ell,J}$, respectively. Using 2 DOF for $\Gamma_{\mathrm{n}}^{\ell,J}$ follows the recommendation from Ref. [9] since the spin of ^{59}Ni is 3/2. The other values can be considered somewhat conservative, since radiative capture proceeds through "many" channels[4] and 1 is the minimum possible DOF (lower DOF gives larger spread in the sampled values).

The first step in the ladder requires special care, because it is desired to sample only in the desired energy range, but starting from a resonance which is located below or at the lower boundary of the range. Therefore, the distribution should be set to zero below the energy range, and could be renormalized to ensure an integral of 1. However, there is a risk that the highest energy resonance for the considered (ℓ, J) is not reported among the measured resonances (or that the approximation to use a Wigner distribution for the levels is imprecise), with the possible result that the distribution becomes undefined; *i.e.*, all the probability mass of the original Wigner distribution is outside the energy range. In such cases, the starting position is first sampled uniformly in the range $\left[E_{\mathrm{URR},0} - 2D^{\ell,J}(E_{\mathrm{URR},0}), E_{\mathrm{URR},0}\right]$, that is, assuming that there is an unmeasured level consistent with the average level spacing and the Wigner distribution, but without any other information of its position.

3. *Sampling bound resonances*

Bound resonances (resonances at negative energies) are not measured directly but impact the thermal cross sections. In this work, positions and widths of such resonances are sampled, and later the widths are adjusted to match the thermal cross sections as described in Sec. III B.

The sampling is very similar to the sampling in the URR described in Sec. III A 2, except that the ladder now starts at the resonance with the lowest energy for the considered (ℓ, J) and decreases in energy. The upper boundary in this case, $E = 0$, is treated as the lower boundary in Sec. III A 2. The average level spacings and widths are obtained by forcing TALYS to return URR parameters for $E = 10^{-4}$ eV ("almost zero"). Again, the same TALYS parameters are used as for the TENDL-2015 random files.

For each (ℓ, J), two bound resonances are sampled.

[3] The URR parameters are linearly interpolated using a fine energy grid. This is judged to have a very small impact, because the parameters vary slowly with energy.

[4] In Ref. [9], the DOF for $\Gamma_\gamma^{\ell,J}$ is recommended to be approximated by infinity, but this is the opposite of conservative.

B. Adjustment to the thermal cross sections

For each random set of nuclear data, the thermal cross sections have been sampled as described in Sec. II, and resonance parameters have been obtained as in Sec. III A, sampling from both experimental data and output from TALYS using randomly sampled parameters. As detailed below, these two bodies of information are combined by adjusting the widths of the (sampled) bound resonances, such that the thermal cross sections reconstructed from the parameters agree with what was obtained from sampling from experimental data.

The adjustment is carried out by multiplying the widths for the same channel (n, γ, α or p) by a common factor ζ_r for all bound resonances (r can be replaced by n, γ, α or p). The multiplication factors are found by numerical root-finding in an iterative procedure over the widths:

1. The Γ_n are adjusted until (n,el) agrees
2. The Γ_γ are adjusted until (n,γ) agrees
3. The Γ_α are adjusted until (n,α) agrees
4. The Γ_p are adjusted until (n,p) agrees
5. Terminate iteration if all thermal cross sections agree within 0.1 mb (less than 0.01%). Otherwise, go back to point 1.

The procedure is repeated until all the thermal cross sections agree within 0.1 mb (less than 0.01%).

As a first attempt, the root-finding is carried out using the function `optimize.newton` of the Python [28] package `scipy` [29], with $\zeta_\mathrm{r} = 1$ as starting guess. If the `optimize.newton` does not converge (to a non-negative solution), another and more safe attempt is made. This starts with a search for a sign change (of the function to find the zero for) between $\zeta_\mathrm{r} = 0$ and $\zeta_\mathrm{r} = 512$, starting with $\zeta = 1$ and then a stepwise increase of the interval length with a factor of 2. If an interval with a sign change is found, the root finding function `optimize.brentq` (also from `scipy`) is used.

If this procedure does not find a root, it is concluded that the combination of the rest of the random file and the simulated thermal cross sections are incompatible ("unphysical"), and the thermal cross sections are simulated again, as motivated in Sec. II B. It turns out that about 95% of the samplings are redrawn. Thus, this approach can impact the distribution of the thermal cross sections and the other uncertain parameters significantly. Under the assumption that the incompatible sets of data are unphysical, this is a desired behavior of the method. For example, many combinations of low energy resonance parameters, bound levels, and thermal cross sections cannot combine. It is *possible* that the root-finding fails to converge even if there is a physically consistent solution, but we believe that the combination of root-finding routines described above is robust.

If it would be undesired to let some set of data to be affected by the others, one can restrain from redrawing that set of data if the convergence fails.

C. Energy grid for pointwise cross sections

The (n,α) and (n,p) cross sections are reconstructed from the resonance parameters obtained above and are stored as pointwise cross sections. This is done because the format does not allow for storing them as resonance parameters without moving to the "`LRF=7`" format [9], which would demand a more detailed knowledge than found in the available experimental data (or wild assumptions).

To follow the convention used in the TENDL data (see Sec. III D), linear-linear interpolation is used (even if log-log interpolation can be more efficient for lower energies). The energy grid used for the pointwise representation is set up starting from a coarse grid including the resonance energies. It is then progressively made denser by introducing new grid points between old grid points, if this is necessary to reach certain tolerances for the pointwise interpolation error and an "integral" interpolation error. The integral interpolation error is defined as the error in

$$\mathcal{I} = \int_0^\infty \frac{\varsigma(E)}{E}\,\mathrm{d}E. \tag{10}$$

The interpolation error of this integral can be approximated by

$$\Delta\mathcal{I} \approx \frac{1}{2}\sum_{i=1}^{N}\frac{\Delta\varsigma(E_i)\Delta E_i}{E_i} \leq \frac{N}{2}\max\left|\frac{\Delta\varsigma(E_i)\Delta E_i}{E_i}\right| \tag{11}$$

where ΔE_i is the length of the energy interval associated with the energy point E_i, and $\Delta\varsigma(E_i)$ is the interpolation error in $\varsigma(E_i)$. Thus, the integral interpolation error meets the relative error tolerance $t_\mathcal{I}$ if

$$|\Delta\varsigma(E_i)| \leq \frac{2E_i\mathcal{I}t_\mathcal{I}}{N\Delta E_i}. \tag{12}$$

The grid is densified until the pointwise interpolation error is less than 1% and the integral interpolation error is less than $t_\mathcal{I} = 0.01\%$. For the random ND sets in this work, the procedure results in grids that contain between 3000 and 8700 points.

D. Assembling complete random ENDF files

For each random set of ND, the resonance energies E_λ, and the widths Γ_tot, Γ_n and Γ_γ are stored in `MF=2` of the ENDF-6 format [9], using `LRF=2` (Multi-Level Breit-Wigner). The randomly generated URR parameters mentioned in the beginning of Sec. III A 2 are also added to `MF=2`, with `LRP=LSSF=1` such that they are only used for self-shielding.

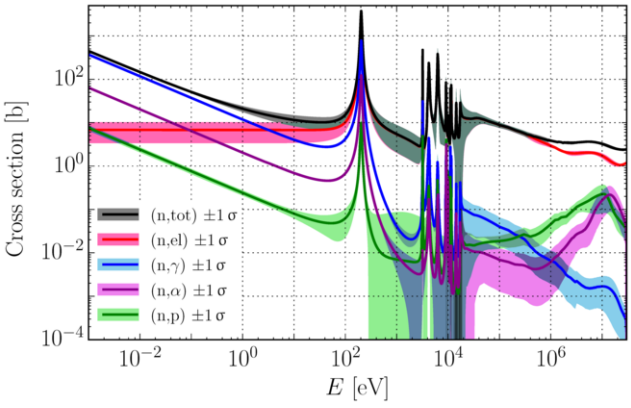

FIG. 4: (Color online) The cross sections resulting from this study as functions of energy from E = 1 meV to E = 30 MeV, with a one standard deviation uncertainty band.

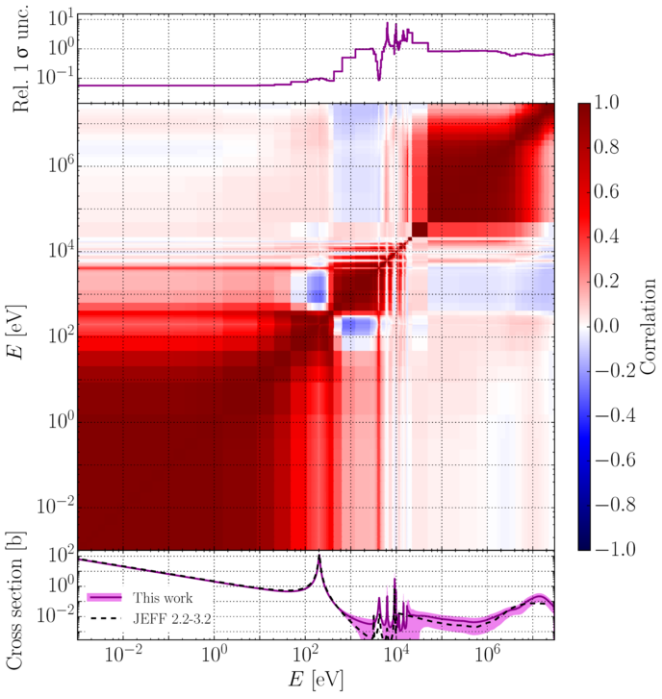

FIG. 5: (Color online) The energy-energy covariance matrix for the (n,α) cross section resulting from this study, illustrated by the corresponding correlation matrix and the relative uncertainty (one standard deviation) as a function of energy. The cross section itself is also plotted as a function of energy and compared to JEFF 2.2-3.2.

The (n,α) and (n,p) cross sections are reconstructed onto the energy grid described in Sec. III C and stored in `MF=3`. All (infinite-dilute) cross sections at energies between 38.9 keV and 200 MeV are taken from the random files of TENDL-2015 and are also put in `MF=3`.

Finally, the remainders of the random files (everything except cross sections and resonance parameters) are copied from the random files of TENDL-2015. Note that for each random ND file, the same TALYS parameters are used in Sec. III as in TENDL-2015.

E. Resulting cross sections

The resulting cross sections and their uncertainties are illustrated in Fig. 4, where smoothing is applied in the part of the URR where resonances are sampled (see Sec. V A). The cross sections show a rather expected behavior: for lower energies, the non-elastic cross sections show a $1/\sqrt{E}$ dependence and the elastic cross section has a constant value. This is followed by a few resolved resonances between about 200 eV and 20 keV, and above these energies, the cross sections show a smooth behavior (in the URR because they are smoothed). The relative uncertainties are smaller for lower energies, while the uncertainty bands can span orders of magnitude for higher energies, in particular in the valleys between resonances (where the *absolute* uncertainty nevertheless may be small).

For the (n,α) cross section, the energy-energy covariance matrix is also illustrated, in Fig. 5, by showing the relative uncertainty as a function of energy and the energy-energy correlation matrix. For the covariance, a 199 group structure is used, see Sec. V B. The figure also shows the cross section itself compared to JEFF 2.2-3.2 (which is copied to ENDF/B-VII.1).

One can tell that the relative uncertainty for (n,α) is rather constant, about 5%, up to a few tens of keV; this is determined by the thermal cross section uncertainty. The uncertainty increases for the RRR where it fluctuates with the resonances and ranges from about 10% to several hundred %. For higher energies, the uncertainty is more steady at about 80%, agreeing well with what is found to be the "global (n,α) uncertainty" in Ref. [30]. If one studies the relative uncertainties for the other partial cross sections, quite similar behavior is seen: a constant value determined by the thermal cross section uncertainty below the resonance range, greater fluctuating values in the resonance range, and rather constant values for higher energies, agreeing with the "global" uncertainties in Ref. [30].

The correlation matrix has four blocks with strong correlation:

1. Up to and including the resonance at 203.4 eV, indicating that this resonance dominates the lower energy cross section.

2. The rest of the RRR (up to 17.2 keV); somewhat fluctuating.

3. The part of the URR with sampled resonances (up to 3.89 keV); the used URR parameters are the same for each random set of ND.

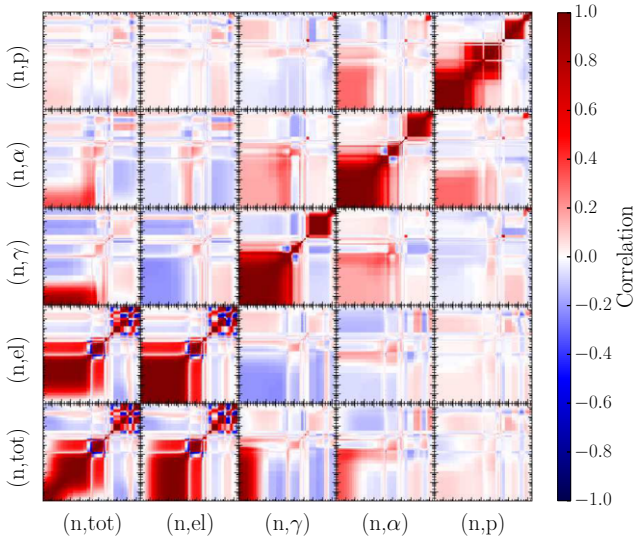

FIG. 6: (Color online) Cross-channel energy-energy correlation matrix. The energy axes are unlabeled because of the limited space, but they are logarithmically spaced between 1 meV and 30 MeV, just as in Fig. 5. Note that other reaction channels than those presented in the figure also have cross-channel correlations.

4. Higher energies; model correlations from TALYS.

Note that there are correlations *between* the different blocks described above, too, particularly significant between the latter two blocks (because the used URR parameters are obtained from the same TALYS runs). Note also the negative correlations occurring between resonance peaks and valleys. The correlation matrices for the different partial cross sections follow quite similar patterns (not illustrated in detail).

There are also strong cross-channel correlations, illustrated in Fig. 6. The correlations arise from the correlations between thermal cross sections, but also from the resonance parameters, the nuclear reaction models, and how all these combine.

It can be noted that, under the assumption of a multivariate Gaussian, a sample correlation ρ which satisfies

$$|\rho| < \rho_{\text{signif.}} = \frac{t_{\alpha/2}(n-2)}{\sqrt{n-2-t_{\alpha/2}(n-2)}}, \tag{13}$$

where n is the sample size and $t_\alpha(n-2)$ is the α-quantile of the Student's t-distribution with $n-2$ degrees of freedom, is insignificantly different from zero with significance level $1-\alpha$ [31]. That is, the (possible) null hypothesis that the true correlation is zero cannot be rejected. In this case, $n = 300$, which yields $t_{\alpha/2}(n-2) = 1.97$ (if $\alpha = 5\%$), in turn giving $\rho_{\text{signif.}} = 11\%$. Thus, assuming the null hypohesis that the true correlation is zero between two points, this null hypothesis cannot be rejected if the magnitude of the observed correlation is less than 11% (with a significance level of 95%). Informally, one could say that sample correlations ρ such that $|\rho| < \rho_{\text{signif.}}$ very well may be observed "by chance". This does not mean that the correlation *is* zero; it could also be that the test is too weak, *i.e.*, that the true correlation is too small to be "detected" with such a sample size.

It can be mentioned that the distribution of the cross sections is non-normal. Studying the marginal distributions of the different cross sections per energy, it is found that the p-value for normality (using the Shapiro-Wilks test) is very small for most cross sections at most energies. At the thermal point, normality can be rejected for (n,el), (n,α), and (n,p), which have p-values less than 0.01 and skewness values of $0.97, 0.43$ and 0.47, respectively.

The (n,α) cross section of this work agrees rather well ($\lesssim 1\,\sigma$ difference) with that in JEFF 2.2-3.2 in the fast range and for energies below the third resonance. This third resonance is smaller for JEFF and outside the uncertainty band. For the following resonances represented in JEFF, the central curves differ but within the uncertainty. The JEFF curve becomes smooth at lower energies than in this work, which gives a certain disagreement. The overall agreement is similar or better for the other channels, except for (n,tot) and (n,p) in the fast range.

F. Resulting resonance parameters

The resonance parameters resulting from the above procedure are tabulated, along with Harvey's quoted resonance parameters, in Table IV. Some alternative information, such as $\Gamma_n\Gamma_\alpha/\Gamma_{\text{tot}}$, is also tabulated in some cases for comparison with Harvey's quoted values. Note that only mean values and standard deviations are tabulated; correlations and higher moments are not looked into, but are nevertheless represented in the distribution of the parameters in the random sets of nuclear data.

In most cases, the values of this work agree well (within the sampling uncertainty) with Harvey's quoted values. The most distinguishing exception is the parameters of the lowest energy resonance: all expected values and almost all standard deviations deviate more than three sampling uncertainty standard deviations. This can be explained by the rejection of samples which fail to reproduce the thermal cross sections; the lowest energy resonance impacts the thermal cross sections substantially and the thermal cross sections seem to indicate generally smaller resonance parameters than Harvey's values for this resonance. A similar reasoning could help explain the (less distinguished) deviations for the resonance at 4211 eV.

We consider it desirable that the thermal cross sections impact the resonance parameters (and vice versa), since we obtain a combination of both sources of information. If this would not be desired, the resonance parameters can be held fixed when redrawing the other information (see Sec. III B).

Even in the cases with a deviation which is large com-

pared to the *sampling* uncertainty, the deviations between the parameters of this work and Harvey's are small compared to the actual uncertainty of the *parameters*. Only in one case, Γ_p for the 203.4 eV resonance, the one standard deviation uncertainties do not overlap.

In some other cases, the standard deviations are greater for this work; this is not very surprising since approximative systematic uncertainties have been added to the resonance parameters. Further, it can be noted that $\langle\Gamma_p\rangle$ is significantly less in this work for a couple of resonances when Γ_{tot} (and not Γ_n) is given by Harvey. This is probably because Γ_{tot} limits the other widths. Finally, the values for $\langle\Gamma_\alpha\Gamma_n/\Gamma_{tot}\rangle$ disagree for the highest energy resonance. This can be explained by the condition that the total width cannot be less than any sum of partial widths, which yields a lower limit for Γ_n (details in Appendix C).

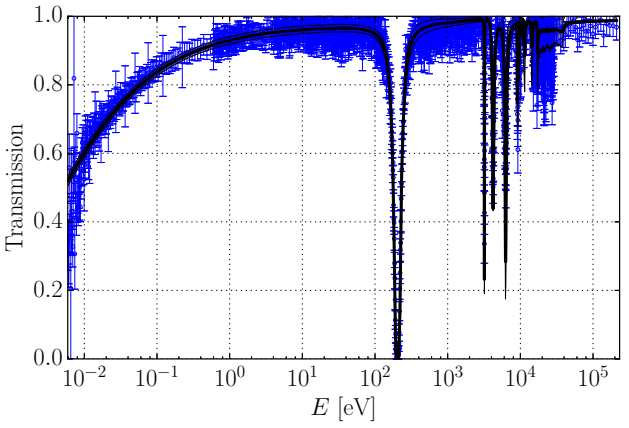

FIG. 7: (Color online) Comparison between the evaluation and (n,tot) data from EXFOR subentry 10680010, in transmission space.

IV. INTEGRITY CHECKS OF THE RESULTING DATA

A. Using Harvey's and Raman's (n,tot) data

In EXFOR, there are 9 EXFOR subentries for Harvey/Raman from 1975 to 1976. Because of lacking documentation, we assume that this data is involved in determining the resonance parameters that are used in this work. Therefore, we do not infer much information from this (n,tot) data, except for the conclusion that the resonances at 1333 eV and 1742 eV are weak (see the caption of Table IV). Instead, the data is used to verify the distribution of the cross sections obtained in this work.

The comparison between the evaluated cross sections and the experimental data is performed in "transmission space", *i.e.*, the evaluated as well as the experimental data is transformed using

$$T(E) = e^{-Nd\varsigma_{tot}(E)}, \tag{14}$$

where T is the transmission and Nd is the number of nuclides per area, which is provided in the EXFOR entries.

For the evaluation, T is computed for each random set of nuclear data, such that a distribution for T is obtained, from which a mean vector $\mathbf{T}_{eval}$ and a covariance matrix $\mathbf{C}_{eval}$ can be computed. The transmission is computed on the energy grid of the experimental data.

For the experimental data, sampled curves for T are also obtained, by sampling from the experimental uncertainty of ς_{tot} and from an assumed uncertainty of 5% on Nd (same for all energies). A mean vector $\mathbf{T}_{exp}$ and a covariance matrix $\mathbf{C}_{exp}$ are computed. When computing $\mathbf{C}_{exp}$, uncertainties as for Harvey's (n,tot) cross section data in Table IV are added.

As an example, the agreement between the evaluation and the experimental set from EXFOR subentry 10680010 is seen in Fig. 7. The evaluation appears to follow the experimental data, and this is confirmed by a reduced χ^2 of 1.00.

Using the mean values and covariance matrices obtained for the evaluation and the experimental data, the generalized χ^2 is computed for each EXFOR subentry to compare their agreement, according to

$$\chi^2 = \frac{1}{2}(\mathbf{T}_{eval}-\mathbf{T}_{exp})^T(\mathbf{C}_{eval}+\mathbf{C}_{exp})^{-1}(\mathbf{T}_{eval}-\mathbf{T}_{exp}). \tag{15}$$

More specifically, we consider the reduced χ^2, $\chi^2_{red} = \chi^2/m$, where m is the number of experimental points. The reduced χ^2 should be distributed around 1, assuming that the evaluation is not fit to this data. We also consider the corresponding p-values which makes better use of the distribution for the χ^2-statistic.

The computation of the χ^2 is also done using $\mathbf{C}_{eval} = 0$, to enable a comparison of the agreement of the mean transmission to that of JEFF 2.2-3.2 (which doesn't provide uncertainties).

The resulting χ^2_{red} values are seen in the first part of Table V. The number of degrees of freedom is so large in all these cases that the corresponding p-values are either practically zero (if $\chi^2_{red} > 1$) or practically one (if $\chi^2_{red} < 1$). As can be seen, three of the EXFOR subentries (13774004, 13775002 and 13775003; all from 1975) agree very poorly with this evaluation, but also to JEFF 2.2-3.2. Inspecting these subentries further, one finds that they disagree very strongly with each other and the other 6 subentries, suggesting that they are erroneous, or erroneously reported. In Ref. [32] (one of the limited references to the considered Harvey/Raman data) an error in sample mass is mentioned. This error could explain some of this dubious data.

For the other 6 subentries, $0.30 \leq \chi^2_{red} \leq 1.00$, indicating an excellent agreement. The agreement can be interpreted as "too good", but this is expected since the considered data is suspected to have been used to determine the resonance parameters which have provided a base for the resonance parameters in this work; *i.e.*,

TABLE V: The reduced χ^2 values obtained when comparing the different experimental (n,tot) sets to this evaluation (with and without covariances) and JEFF 2.2-3.2.

				Reduced χ^2		
				This work		JEFF 2.2-3.2
1st author	Year	EXFOR ID	Energy range [eV]	Incl. eval. cov	Excl. eval. cov	
Raman	1975	13774002	$.329 - 1.48 \cdot 10^5$	0.56	1.40	0.68
Raman	1975	13774003	$.243 - 1.55 \cdot 10^4$	0.30	0.47	0.45
Raman	1975	13774004	$53.5 - 495.$	3.9	5.9	6.4
Harvey	1975	13775002	$4.59 - 2.19 \cdot 10^5$	6.1	17.5	16.4
Harvey	1975	13775003	$43.9 - 2.19 \cdot 10^5$	11.5	47	39
Harvey	1975	13875002	$.00662 - 1.48 \cdot 10^5$	0.73	0.85	0.90
Harvey	1975	13875003	$.00662 - 1.48 \cdot 10^5$	0.89	1.10	1.17
Harvey	1976	10680009	$1.98 - 2.02 \cdot 10^5$	0.89	2.4	1.28
Harvey	1976	10680010	$.00592 - 2.11 \cdot 10^5$	1.00	1.99	1.27
Thermal cross section exp.				0.44	0.45	1.12

a very good agreement is to be expected. Hence, the (n,tot) data is not perfectly suitable as validation data, but is rather used for an integrity check.

When comparing only the central curve of the evaluation to the experimental data, the agreement is worse; many χ^2_{red}-values are substantially greater than one. This is not surprising, since an evaluated uncertainty of zero is equivalent to assuming that the evaluation perfectly represents the truth. Nevertheless, the agreement for the central curve is in three cases substantially worse, but never much better, than for JEFF 2.2-3.2. It could be that the JEFF cross sections are adjusted to some of this total cross section data, and that it is based more exclusively on this Harvey/Raman (n,tot) data than the cross sections of this work, the latter also taking several different thermal experiments into account. Additional fitting to the (n,tot) data could lead to unfairly reduced uncertainties, but also to a larger deviation to the other cross sections.

B. Using thermal cross section data

On the last row of Table V, there are values for χ^2_{red} when doing the same comparison as in Sec. IV A, but for the thermal cross section data considered in Sec. II. The experimental data is taken as it is after the analysis of the individual experiments, but without introducing physical constraints (corresponding to part *ii* in Table III).

For the Ashgar data, (n,α) of the evaluation is compared to the sum of (n,α_0) and (n,α_1), and (n,p) is compared to the sum of (n,p_0) and (n,p_1). In the other cases, (n,α) is compared to (n,α_0), and (n,p) is compared to (n,p_0). This leaves 10 points for comparison. The experimental covariance matrix is obtained as the sample covariance for these experimental points, sampled according to Sec. II B 2.

In this case, the difference between the results of this evaluation, when including or excluding the covariance of the evaluation, is small. This is because the uncertainty of the experiments is substantially greater; it is expected that the evaluation has smaller uncertainty since it, in a sense, is a fit to the experimental data. Again, the χ^2_{red} values are "too" low because we have made use of this data in the evaluation. The agreement between JEFF 2.2-3.2 and the thermal cross section experiments is worse (but not bad), which is not surprising since JEFF 2.2-3.2 is not adjusted directly to this set of evaluated experimental data.

In the computation of χ^2_{red}, no reduction of the degrees of freedom due to fitting has been performed, since it is not well-defined for non-linear models. However, if we consider it as we have fitted 4 parameters (the four partial thermal cross sections), the χ^2_{red} comparing this evaluation to the thermal cross section data is 0.73, corresponding to a p-value of 0.63.

Note that a comparison to 10 experimental points constitutes a rather weak statistical test; with a 95% confidence level, insignificant results are obtained for $0.32 < \chi^2_{\text{red}} < 2.05$ and $0.21 < \chi^2_{\text{red}} < 2.41$, assuming 10 or 6 degrees of freedom, respectively. Thus, relatively large deviations would be necessary for a disagreement to be detected.

V. FROM RANDOM FILES TO ONE FILE WITH COVARIANCES

It is straightforward to use the random files produced within this evaluation for Monte Carlo uncertainty propagation, since the distribution of the ND is intended to describe the probability density of the considered ND, given the current state of knowledge. However, ND uncertainty propagation is still dominated by linear error propagation, and the ND uncertainty representation is still dominated by covariance matrices. Therefore, the information contained in the random ND files is condensed (with certain information loss) into one single ENDF file with covariances. Such a file is now part of a beta version of JEFF 3.3.

A. Smoothing sampled URR and incompletely reported resonances

In the part of the URR where resonances are sampled, we do not know the positions of the resonances and the best guesses for expected cross sections should be a smooth function of energy; the resulting mean curve would also be smooth if a large enough sample size was used. However, due to the finite sample size, a simple mean (on some grid) will cause the cross section curve to be very ragged in this region. This would not be physically motivated, but just a result of random fluctuations. Therefore, Gaussian kernel smoothing is applied to the mean curve in this region. The standard deviation of the Gaussian kernel is set to the maximum of the level spacings (with respect to the quantum numbers) according to the URR parameters provided by TALYS for the nominal set of parameters in TENDL-2015, and the kernel is cut off at 3 standard deviations. Close to the boundary of unsmoothed energies, the kernel's standard deviation is decreased such that the kernel does not reach outside the smoothed region.

The same smoothing methodology is applied to resonance peaks for resonances that are incompletely reported and, therefore, have sampled quantum numbers resulting in very varying shapes of the resonances. Some peaks are substantially more narrow than the uncertainty of the position of the resonance, giving rise to ragged peaks of the average cross section. Again, this shape is unphysical. The smoothing is applied for energies $E_\lambda \pm 4\Delta E_\lambda$, where E_λ is the expected resonance energy and ΔE_λ its standard deviation. The kernel standard deviation equals ΔE_λ (decreased towards the boundaries as described above).

B. Covariances

1. Cross sections

The cross sections (including reconstructed resolved resonance parameters) of each random set of ND is collapsed into a 199 group structure, where the group limits are set up at the energy grid points such that the number of grid points in each group is as constant as possible. Since the grid is adapted to the structure of the cross section to fulfill certain interpolation error tolerances, this yields a group structure which captures the particular cross section structure of ^{59}Ni.

Then, the sample covariance is computed between each such energy group (when non-zero) for all channels (`MT` numbers) present in the file except inelastic scattering to excited levels above the 20$^{\text{th}}$. The upper triangle of this covariance matrix is then stored in submatrices representing one or two channels in `MF=32` following the ENDF-6 format [9], using the format flags `LB=5` and `LB=6`. An additional component is added to the diagonal of the covariance matrix using `LB=8`, increasing the uncorrelated variance by 1%. This is in line with a recommendation in Ref. [9]. The resulting covariance matrix is positive definite (even numerically).

2. URR parameters

Due to format limitations, covariances for the URR parameters can only be given for the mean URR parameters. Therefore, the mean URR parameters with respect to energy are computed using the trapezoid integration rule for each random set of ND (in which the URR parameters originate from the different TALYS runs). Then, the sample covariance matrix for these mean parameters is computed and stored into `MF=32`.

3. Other covariance information

The other covariance information is copied from TENDL-2015. This data has its origin in the same distribution of TALYS parameters, but the correlation between different parts of the data is lost; this is, however, impossible to avoid due to format limitations. Moving from random files to one file with covariances, the correlation between URR parameters and cross sections is also lost, as well as higher moments of the distribution and structure on a finer scale than the group structure.

C. Representing the mean cross sections with resonance parameters and background cross sections

In each of the random ENDF files, the (n,tot), (n,el) and (n,γ) cross sections for $E < 38.9$ keV are represented entirely by resonance parameters (while (n,α) and (n,p) are represented by pointwise data). When condensing the random files to one file with covariances, the central cross section values should be the expected values of the respective cross sections. At the same time, it is desirable to represent the data using resonance parameters, as these can be used for computing self-shielding factors by some codes. However, the mean values of the resonance parameters will not in general reproduce the mean values of the cross sections. In particular, this becomes a problem for parameters with very large uncertainties, *e.g.*, resonances positioned with a random ladder. Moreover, some of the resonances have sampled quantum numbers, which cannot be represented adequately by mean resonance parameters.

This dilemma can be reasonably well solved by giving the mean parameters for the resonances which are completely reported (in `MF=2`), combined with a correcting background cross section (in `MF=3`) which accounts for the resonances with sampled positions or quantum numbers, as well as the deviation between the mean of the cross sections and the cross sections using the mean parameters. That is, the background cross section ς_{bg} is

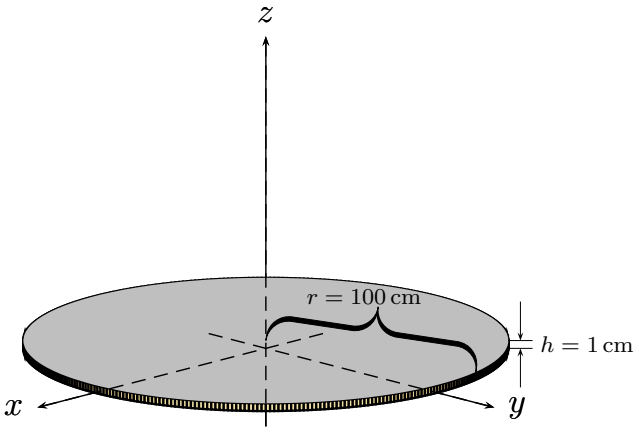

FIG. 8: (Color online) The geometry used in the MCNP model.

TABLE VI: The elemental composition used for the stainless steel.

	Fe	Cr	Ni	Mn
Mass %	69.5	19	9.5	2

defined by

$$\varsigma_{\text{bg}}(E) = \bar{\varsigma}(E) - \varsigma_{\bar{\mathbf{p}}_{\text{complete}}}(E)\,, \tag{16}$$

where $\bar{\varsigma}(E)$ is the mean cross section and $\varsigma_{\bar{\mathbf{p}}_{\text{complete}}}(E)$ is the cross section reconstructed from the mean of the completely reported parameters.

VI. USING THE RANDOM FILES FOR HELIUM PRODUCTION IN A THERMAL SPECTRUM

A. The model

To test the random ND files produced in Sec. III D, and to get an indication on how the simulated distribution of the thermal cross sections affects the production of helium gas in a thermal reactor, the random files are used in a simple MCNP6 [33] model.

The model consists of a "pancake-shaped" cylinder of stainless steel, with height (thickness) 1 cm and a radius of 1 m, as illustrated in Fig. 8. The elemental stainless steel composition is specified in Table VI. On one side of the cylinder (the plane $z = 0$ in Fig. 8), there is a surface source[5] with neutrons from a "typical" spectrum at 1/4 of the thickness of the pressure vessel, from Ref. [34]. In each run, 10^7 neutrons are simulated.

[5] The distribution of the direction of the surface source is the default of MCNP 6, *i.e.*, a cosine distribution.

TABLE VII: The isotopic nickel compositions (mass %) used for natural nickel and modified nickel (representing the ^{59}Ni peak), respectively.

	^{58}Ni	^{59}Ni	^{60}Ni	^{61}Ni	^{62}Ni	^{64}Ni
Natural	68.1	-	26.2	1.14	3.63	0.926
Modified	57.8	3.06	32.1	1.39	4.45	1.13

The model is run once with natural nickel, and then n times (once for each random file) with the nickel content modified according to Table VII, where the ^{58}Ni and ^{59}Ni values approximately correspond to the values in the ^{59}Ni peak in Ref. [3]. The distribution of the (n,α) reaction rate with the modified nickel is compared to the value obtained for the natural nickel. Note that other nuclides and elements than ^{59}Ni can contribute to this reaction rate.

The random ENDF files are processed into ACE files[6] using NJOY-99.336 and a temperature of 293 K. For other nuclides than ^{59}Ni, data from ENDF/B.VII.1 for 293 K is used.

B. Results

Figure Fig. 9 shows the distribution (using the ^{59}Ni random files) for the ratio of the (n,α) reaction rate using modified nickel over the (n,α) reaction rate using natural nickel. In other words, the figure shows the distribution for how much the (n,α) rate increases with the ^{59}Ni-containing nickel compared to natural nickel. The figure also shows the PDF of a normal distribution with the same mean and standard deviation. The expected value is estimated to 5.19(2), and the standard deviation due to ND uncertainty is estimated to 0.28(1), or 5.4(2)%.[7] Thus, we expect more than a five-fold increase of the (n,α) rate at the ^{59}Ni-peak compared to natural nickel, but it may also be up to six-fold.

One may note that the relative uncertainty of the (n,α) reaction rate is slightly less than that of the thermal (n,α) cross section, which is 5.6(2)%. This may be surprising since the relative (n,α) uncertainty is greater for higher energies and the energy-energy correlations are mostly positive. However, only about 4/5 of the (n,α) reactions are in ^{59}Ni (the *increase* is approximately five-fold; the rest is in other nuclides for fast neutrons). Thus, the relative uncertainty of 5.2(2)% corresponds to a somewhat larger uncertainty relative to the (n,α) reaction rate in ^{59}Ni *only*.

[6] File format used by MCNP, ACE stands for "A Compact ENDF".

[7] The statistical uncertainty from the Monte Carlo code is estimated to 0.22%, so even if this is taken into account as described in Refs. [23, 35], it does not make any practical difference for the results.

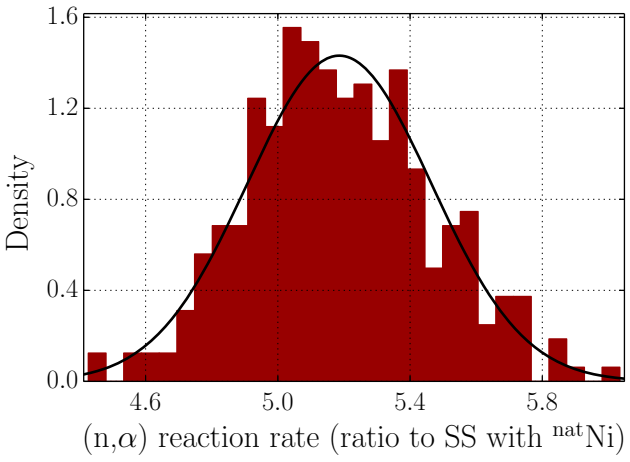

FIG. 9: (Color online) Observed distribution for the ratio of the (n,α) rate for modified nickel (containing ^{59}Ni) and natural nickel.

VII. CONCLUSIONS

^{59}Ni has been evaluated, including uncertainties, using a novel approach to nuclear data evaluation. This combines the sampling of errors in thermal cross section experiments with resonance parameters and nuclear physics models as implemented in TALYS.

In particular, the thermal (n,α), (n,p), (n,γ) and (n,tot) cross sections have been carefully evaluated. The random and different systematic errors of the experiments have been sampled and combined with "physical" constraints, *e.g.*, that the (n,el) cross section must be non-negative. In this way, a new estimate for the *joint distribution* of the thermal cross sections has been obtained, including expected values and standard deviations as well as correlations between the different cross sections. The expected values and standard deviations differ from, but are consistent with, the values quoted in Mughabghab [2] and the evaluation contained in JEFF 2.2-3.2 (which is copied into ENDF/B-VII.1). In particular, the (n,α) cross section is estimated to $(12.73(4) \pm 0.71(3))$ b, compared to (12.3 ± 0.6) b in the work of Mughabghab, and 13.5 b which is found in JEFF.

The obtained distribution for the thermal cross sections have been combined with resonance parameters, and with TALYS 1.8 results using the parameter distribution of TENDL-2015. The parameters of the bound resonances have been adjusted to match the distribution of the thermal cross sections. The procedure yields correlations within, and between, the different parts which reflect how the evaluation is done. The resulting ND is stored as 300 random ENDF files, but also condensed into one ENDF file with covariance information.

The random ENDF files have been processed into ACE files and then used to propagate the nuclear data uncertainties of ^{59}Ni to a simple application: by using MCNP6, the (n,α) rate in stainless steel in a spectrum in the pressure vessel of a light water reactor is studied. The increase of the (n,α) rate due to ^{59}Ni at a certain time in the reactor vessel compared to fresh stainless steel is approximately five-fold, with an uncertainty due to ^{59}Ni data of 5.2(2)%.

It may finally be mentioned that even though this work considers ^{59}Ni, there is no hinder for the methodology to be applied to other nuclides, as well.

Acknowledgements

Funding for this work was received from Swedish Center for Nuclear Technology SKC through Mabil, from Uppsala University, and from Nuclear Research and Consultancy Group NRG.

Special thanks to Jean-Cristophe Sublet (UKAEA, Abingdon, UK) for discussions on the ENDF format, to Denise Neudecker (LANL, Los Alamos, NM, USA) for discussions on experimental uncertainties, and to Arjan J. Koning (IAEA-NDS, Vienna, Austria) for general discussions on nuclear data uncertainties and TMC.

APPENDIX A: ANALYSIS OF THERMAL CROSS SECTION EXPERIMENTS

Based on Sec. II A, the available experiments are analyzed as detailed below, experiment by experiment. The resulting uncertainty components are summarized in Table III, and the difference between the original and evaluated experimental information is visualized in Fig. 2.

1. Eiland/Kirouac, 1974 [13]

Measured (n,α_0), *i.e.*, (n,α) leaving the recoil nuclide in its ground state, in a thermal spectrum from a graphite-moderated neutron-beryllium source detected with particle track detectors. The experiment actually consists of two sub-experiments; the major differences are ^{59}Ni enrichment and detector efficiency (determined using an americium source).

Both sub-experiments consisted of six measurements, and the standard deviation of each set was used as an estimate of the uncertainty from "all sources of random error", giving $\varsigma_{\text{th.}} = (13.5 \pm 1.8)$ b and $\varsigma_{\text{th.}} = (13.7 \pm 0.6)$ b for sub-experiment 1 and 2, respectively. The flux was determined using activation of gold via the ^{197}Au(n,γ) reaction. This determination was estimated to have a 3.6 % systematic uncertainty. The americium source strength used to determine the detector efficiency was estimated to have an uncertainty of 2.5 % from statistics. Using these systematic uncertainties (assuming all other uncertainties are random) and taking the weighted average of the two sub-experiments, they quote $\varsigma_{\text{th.}} = (13.7 \pm 0.6 \text{ (random)} \pm 0.6 \text{ (systematic)}) \text{ b}$.

In practice, the second sub-experiment and its estimate of random uncertainty dominate completely, and therefore only this sub-experiment is analyzed further. For each of the six measurements, a new estimate of the detector efficiency and the background (as we interpret it) was performed. Three different targets (and estimates of their thickness and density) were used (two measurements with each target). Therefore, uncertainties in all constituents of Eq. (1) are to some degree accounted for. There are however several problems with this estimate:

1. The sample size is small, so the random uncertainty of the uncertainty is large
2. Only three different targets were used, increasing the problem of the small sample size
3. The statistical precision varies (the number of counted tracks varies between 1500 and 4100), so the different measurements cannot be said to come from identically distributed random variables
4. Only two systematic contributions are taken into account – there may be a systematic error in the thickness and density of the Ni target (same type of thickness measurement, same origin of enriched Ni) and also other systematic errors in the determination of the detector efficiency.

The first item is resolved by scaling the uncertainty with the standard deviation of a t-distributed random variable with $5 = 6 - 1$ degrees of freedom, *i.e.*, $\sqrt{5/3} \approx 1.29$ [36], since the t-distribution includes the uncertainty of the sample variance as an estimator of the true variance (also, the t-distribution with 5 degrees of freedom is used when simulating the experiment, see Sec. II B).

The second item is trickier; one can note that a t-distributed random variable with $2 = 3 - 1$ degrees of freedom has an infinite variance; therefore, it is unsatisfactory to include this uncertainty in the random uncertainty and we add a systematic uncertainty for $\mathcal{N}$ according to Table I, also handling a part of the fourth item above.

Since the solution for the second item can be considered somewhat conservative, and since the counting statistics is dominated by other sources of random variance (at most $1/1500 = (2.6\,\%)^2$ compared to $(1.29 \cdot 0.7/13.7)^2 = (6.6\,\%)^2$), the third item is ignored.

The fourth item was partially resolved already, but we add another systematic uncertainty of 2 % in quadrature to the detector efficiency. This corresponds to the uncertainty of ϵ'/ϵ in Table I, which is reasonable since the detector efficiency is measured for one reaction and used for another. The total systematic detector efficiency uncertainty becomes 3.2 %.

Also, the reported standard deviation for the second sub-experiment (0.6 b) does not agree with the sample standard deviation of the reported measurement results (probably, the authors used the commonly used biased variance estimator $\frac{1}{m}\sum_{i=1}^{m}(x_i - \bar{x})^2$ instead of $\frac{1}{m-1}\sum_{i=1}^{m}(x_i - \bar{x})^2$). We instead use the value 0.695 b which is computed using the unbiased variance estimator.

To summarize, the total uncertainty excluding the flux (and the normalization) is 8.83 %, resulting in an increase by a factor of 1.63 compared to the estimate by Eiland and Kirouac. Thus, we adjust the flux uncertainty to $1.63 \cdot 3.6\,\% = 5.85\,\%$, as discussed in Sec. II A.

We also assume that the flux determination used a value of 98.8 b for ^{197}Au(n,γ) (used in Ref. [12] the year after). This is used to renormalize the cross sections to current standards, as described in Sec. II A.

Eiland and Kirouac also claim that (n,α_0) makes up the whole (n,α) cross section for thermal energies and that (n,α_1) begins to contribute to about 1 % of the cross section above 1 keV, citing a previous article by Kirouac [37], where Hauser-Feshbach formalism was used to estimate the (n,α) cross section. However, the branching ratio into different excited states is not mentioned in the actual reference.

2. Werner/Santry, 1975 [12]

Measured (n,α_0) with 0.0551 eV neutrons from a triple axis crystal spectrometer, detected by a silicon surface-barrier detector. Reports $\varsigma(0.0551\,\text{eV}) = (12.0 \pm 1.2)$ b, and, assuming a $1/v$ dependence of the cross section, $\varsigma_{\text{th.}} = \varsigma(0.0253\,\text{eV}) = (18.0 \pm 1.6)$ b. It is not entirely clear how the authors concluded $\varsigma(0.0253\,\text{eV}) = (18.0 \pm 1.6)$ b, since $12.0\,\text{b} \cdot \sqrt{0.0551/0.0253} = 17.7\,\text{b}$.

The quoted uncertainty is "at 90 % probability", and due to 7.5 % counting statistics and "about 3 % each" for the flux estimate, the detector efficiency and the number of ^{59}Ni atoms in the target. Assuming independence of the four components gives a total relative uncertainty of $\sqrt{7.5^2 + 3 \cdot 3^2}\,\% = 9.1\,\%$ which is rounded off to 1.6 b for $\varsigma_{\text{th.}} = 18.0$ b (how 1.2 b uncertainty is obtained for 12.0 b is unclear). Assuming a normal distribution to translate "at 90 % probability" to one standard deviation uncertainty gives $\varsigma_{\text{th.}} = (18.0 \pm 1.0)$ b

The result is so inconsistent with other results that we assume that an unknown systematic error has had a significant effect, and we disregard this experiment from the analysis.

3. McDonald/Sjöstrand, 1975 [15] (corrected by Ashgar *et al.*, 1977 [16])

Measured (n,α_0) (also reported (n,p$_0$) as a spin-off) using neutron energies of 0.0290, 0.0345 and 0.0421 eV from a double crystal monochromator, using a silicon surface-barrier detector. The measurement was performed relative to the ^{6}Li(n,t) by using both a ^{59}Ni enriched Ni-target (produced in R2 at Studsvik) and a LiF-target. The ratio of the ^{59}Ni(n,α) cross section to the ^{6}Li(n,t) cross section was found to be $(2.37 \pm 0.07) \cdot 10^{-2}$, $(2.36 \pm 0.04) \cdot 10^{-2}$ and $(2.37 \pm 0.08) \cdot 10^{-2}$, respectively,

for the three energies. The quoted uncertainties should include the counting statistics but, according to the experimenters, also the uncertainties arising from variations in the flux, in small alternations in the target position, and electronics, since the procedure was repeated "several times" for each energy, but it is also noted that the "largest contribution to the [random] uncertainty arises from [counting statistics]". The weighted average of the ratios (assuming independence between these parts of the uncertainty) is $(2.364 \pm 0.032) \cdot 10^{-2}$. On top of the "random" uncertainties quoted for the ratios, the authors quote 6 %, 3 % and 2 % for the LiF and Ni target thicknesses and the ^{59}Ni density, respectively.

Assuming $1/v$-dependence in the considered energy range for both ^{59}Ni(n,α) and ^{6}Li(n,t), the authors deduce $\varsigma_{\text{th.}} = 22.2 \pm 1.7$ b using a thermal cross section for ^{6}Li(n,t) of 940 b. However, Ashgar *et al.* [16] (Sjöstrand was one of the co-authors) discovered that the ^{6}Li content of the LiF targets used was "0.5 ± 0.04" times what McDonald and Sjöstrand thought. Since this factor is not explained thoroughly in Ref. [16], 0.5 ± 0.1 is used in this work (20 % uncertainty).

Random uncertainties are in a sense treated by repeating the measurement "several" times, but it is not specified what "several" means (*cf.* A 1), and the authors noted that the quoted random uncertainty was dominated by counting statistics. Therefore, we assume that the random uncertainty only covers counting statistics and use the uncertainties in Table I for the background, ϵ'/ϵ and ϕ'/ϕ.

The derivation of the reported (n,p$_0$) cross section is less well described, but reported as (4 ± 1) b. We use the same correction as above, and the same relative uncertainties except for the background, since it was pointed out in Ref. [16] that it is likely that a contribution from ^{10}B(n,α) due to a boron impurity is included in the value quoted for (n,p$_0$). Therefore, we let the uncertainty of the background equal 50 %.

4. Jurney, 1975

Two values for (n,γ) are reported in EXFOR, namely, (53 ± 4) b and (51 ± 8) b. These values are so much in disagreement with other experiments (both (n,γ) and combinations of (n,tot) and the other channels) such that we completely disregard this experiment. The original publication is not found by the authors of this paper.

5. Harvey, 1975/1976

A series of measurements during 1975 and 1976. The best documentation found is an ORNL progress report from 1976 [32]. In the related EXFOR entries (13875 and 10680), there are several references to "private communication" and one to "Review of ORNL measurements, 1978" (which we did not manage to find). Because of the unwieldy documentation, it is chosen to use the EXFOR entry from 1976 (10680) to avoid any double-counting of experiments.

The measurements cover thermal cross sections (as well as resonance widths) for (n,tot), (n,γ), (n,α_0) and (n,p$_0$). The (n,α_0) and (n,p$_0$) cross section measurements use a thermal spectrum from photons impinging on a water-moderated tantalum target and a diffused-junction silicon detector. The (n,γ) and (n,tot) cross sections were obtained with better resolved energies and a total energy detector and a ^{6}Li glass detector, respectively.

Common for all the measurements is that one uncertainty estimate is given per point, but that the sources of the uncertainties are not given in the found documentation. Therefore, we assume that the quoted uncertainties are random and add systematic uncertainties according to Table I. We let the systematic uncertainties correlate fully for $\mathcal{N}$ and $\mathcal{N}'$ between all reactions, since it is likely that the same target is used. The only mentioning of a monitor cross section is the ^{6}Li(n,t) cross section, which we use for renormalization (assuming that 940 b or 941 b was used as in Ref. [15] and Ref. [16], respectively; the two choices are sampled with equal probability in Sec. III). We also let the uncertainty of the background equal 50 % for the (n,p$_0$) cross section due to the possible problem of a boron impurity just as for the McDonald/Sjöstrand experiment.

For (n,α_0), (n,p$_0$) and (n,γ), values of (11.4 ± 0.8) b, (1.43 ± 0.13) b and (78 ± 8) b are quoted, respectively. The (n,tot) cross section is reported for several energies, however. For low energies, it is assumed that the total cross section follows

$$\varsigma_{\text{tot}}(E) = A + \frac{B}{\sqrt{E}}, \tag{A1}$$

where A and B are constants, *i.e.*, the sum of a constant component (elastic) plus a component following a $1/\sqrt{E}$-behavior (non-elastic). Assuming that the reported uncertainty is random uncertainty, and performing a generalized least squares fit for the expression above (a.k.a. weighted least squares in this special case) for the data for $E \leq 0.13$ eV gives $\varsigma_{\text{th.,tot}} = 92.28 \pm 0.58$ b. The limit 0.13 eV was chosen because an investigation of the (n,γ) cross section in a preliminary result within this work agreed with a $1/\sqrt{E}$ behavior within 0.1 % below this energy. After the fit, systematic uncertainties are added according to the above.

6. Ashgar *et al.*, 1977 [16]

This experiment is not reported to EXFOR. The (n,α_0), (n,α_1), (n,p$_0$) and the (n,p$_1$) cross sections were measured using a thermal spectrum from the "long curved neutron guide" of the Grenoble high flux reactor and a gold-silicon surface barrier detector. The ^{59}Ni target is the same as in the McDonald/Sjöstrand experiment briefly described in A 3. The cross section was measured

relative to the ^{6}Li(n,t) cross section, assumed to be 941 b by the authors.

The authors reported (13.1 ± 1.1) b, (0.188 ± 0.016) b, (1.34 ± 0.18) b and ≤ 0.30 b for (n,α_0), (n,α_1), (n,p$_0$) and (n,p$_1$), respectively. The quoted uncertainties include counting statistics, nickel and lithium target thicknesses and the instability of the neutron beam added quadratically, but their contributions are not given separately except for the Ni target thickness (3 %). The authors claim that the (n,α_0) peak is well separated from the peak from ^{10}B(n,α) mentioned in Appendix A 3.

Since the target is the same as in Appendix A 3, we also add a 2 % uncertainty due to the ^{59}Ni density, and both this uncertainty and the Ni target thickness uncertainty are assumed to be fully correlated to the same uncertainties in the McDonald/Sjöstrand experiment. Since nothing is mentioned regarding detector efficiency and background, the default uncertainties of Table I are used for ϵ'/ϵ and the background. To estimate the correlation between the different reactions properly, the default uncertainty for the Li target thickness is subtracted (in quadrature) from the quoted uncertainty and added separately.

The upper limit for (n,p$_1$) is treated by assuming an expected value of a third of this limit, *i.e.*, 0.10 b and a 100 % uncertainty. Using the sampling methodology in this work, this results in an exponential distribution with expected value 0.10 b. Because of this rough treatment (and the small value giving it minor importance), the uncertainty is assumed uncorrelated to all others.

7. Raman *et al.*, 2004 [17]

Measured the (n,γ) cross section using neutrons in the thermal column of the Los Alamos Omega West Reactor. The value is normalized to the ^{58}Ni(n,γ) cross section value obtained in the same experiment, in turn normalized to the ^{1}H(n,γ) cross section (using a value of 332.6 mb).

The authors quote 73.7 ± 1.8 b for the (n,γ) cross section, and claim that the quoted uncertainty "includes contributions from all sources including the normalization [by ^{58}Ni(n,γ)]". However, what these contributions are, is not easily found from the text. The uncertainties of N and N' are quoted, implying relative uncertainties of $0.4/44.3 \approx 1$ % and $0.4/37.9 \approx 1$ %, respectively. Also, the uncertainty of the monitor cross section (^{58}Ni(n,γ)) is given, implying a relative uncertainty of $0.05/4.13 \approx 1$ %. Summing up these explicitly stated uncertainties, one ends up with 1.4 b. The other constituents of Eq. (3) are assigned uncertainties according to Table I.

Similarly to the reasoning for the flux, we assume that the quoted experimental uncertainty for the ^{58}Ni(n,γ) cross section is as underestimated as the uncertainty of the considered uncertainty (disregarding the normalization). Summing all other uncertainties in quadrature gives us a total uncertainty 3.21 times as large as the quoted uncertainty. Replacing the normalization uncertainty 0.05/4.13 included in the quoted uncertainty with $3.21 \cdot 0.05/4.13$ gives that the combined uncertainty from the originally "included" contributions is 4.43 %.

APPENDIX B: USING BAYES' THEOREM TO MOTIVATE REDRAWING UNPHYSICAL OBSERVATIONS

The experimental information gives us a first estimate of the distribution for the random vector $\boldsymbol{\zeta} = (\zeta_{(\mathrm{n},\alpha)}, \zeta_{(\mathrm{n},\mathrm{p})}, \zeta_{(\mathrm{n},\gamma)}, \zeta_{(\mathrm{n},\mathrm{el})})^{\mathrm{T}}$, where (n,tot) is left out because Eq. (6) makes it obsolete. The interpretation of this random vector is that its probability density describes our knowledge of what the true cross sections are.

Let $\mathcal{A}$ be the set of all $\boldsymbol{\zeta}$ that are physically possible. Bayes' theorem [38] can be written

$$f_{\boldsymbol{\zeta}|\boldsymbol{\zeta}\in\mathcal{A}}(\boldsymbol{\varsigma}) = \frac{P(\boldsymbol{\zeta}\in\mathcal{A}|\boldsymbol{\zeta}=\boldsymbol{\varsigma}) f_{\boldsymbol{\zeta}}(\boldsymbol{\varsigma})}{\int_{\mathbb{R}^m} P(\boldsymbol{\zeta}\in\mathcal{A}|\boldsymbol{\zeta}=\boldsymbol{\varsigma}) f_{\boldsymbol{\zeta}}(\boldsymbol{\varsigma})\,\mathrm{d}\boldsymbol{\varsigma}} = \\ = \begin{cases} \frac{f_{\boldsymbol{\zeta}}(\boldsymbol{\varsigma})}{\int_{\mathcal{A}} f_{\boldsymbol{\zeta}}(\boldsymbol{\varsigma})\,\mathrm{d}\boldsymbol{\varsigma}} & \text{if } \boldsymbol{\varsigma}\in\mathcal{A} \\ 0 & \text{if } \boldsymbol{\varsigma}\notin\mathcal{A}, \end{cases} \tag{B1}$$

where $f_{\boldsymbol{\zeta}}(\boldsymbol{\varsigma})$ is the probability density function (PDF) for $\boldsymbol{\zeta}$ using only the experimental information, $f_{\boldsymbol{\zeta}|\boldsymbol{\zeta}\in\mathcal{A}}(\boldsymbol{\varsigma})$ is the PDF for $\boldsymbol{\zeta}$ given that $\boldsymbol{\zeta}\in\mathcal{A}$, *i.e.*, given that the cross sections must be physically possible, and $P(\boldsymbol{\zeta}\in\mathcal{A}|\boldsymbol{\zeta}=\boldsymbol{\varsigma})$ is the probability that $\boldsymbol{\zeta}\in\mathcal{A}$ given that $\boldsymbol{\zeta}=\boldsymbol{\varsigma}$. Clearly, this probability must be one if $\boldsymbol{\varsigma}\in\mathcal{A}$, and the probability must be zero if $\boldsymbol{\varsigma}\notin\mathcal{A}$.

Assuming that the simulations described above are a reproduction of the experimental knowledge, the simulations yield random observations from $f_{\boldsymbol{\zeta}}(\boldsymbol{\varsigma})$. To obtain observations from $f_{\boldsymbol{\zeta}|\boldsymbol{\zeta}\in\mathcal{A}}(\boldsymbol{\varsigma})$ instead, we can redraw from $f_{\boldsymbol{\zeta}}(\boldsymbol{\varsigma})$ until the criterion $\boldsymbol{\varsigma}\in\mathcal{A}$ is fulfilled, since this will make the probability density vanish outside $\mathcal{A}$ and only renormalize it (such that it remains a probability density at all) in $\mathcal{A}$.

APPENDIX C: SAMPLING MISSING INFORMATION FOR INCOMPLETELY REPORTED RESOLVED RESONANCE PARAMETERS

As can be seen in Table IV, Harvey's resonance parameter data is incomplete in some cases; it is not sufficient to reconstruct cross sections from. For these resonances, the missing information is sampled, and the distributions to sample from are determined using the average level spacings and resonance widths (URR parameters) provided by TALYS. Again, the same TALYS parameters as for the random TENDL-2015 files are used.

We have 5 cases to consider:

1. $\Gamma_\gamma, \Gamma_{\mathrm{tot}}, \Gamma_\alpha$ and Γ_{p} are given (two resonances)

2. Γ_γ and Γ_{tot} are given (two resonances)
3. Γ_γ is given (two resonances)
4. $\frac{\Gamma_\text{n}\Gamma_\alpha}{\Gamma_{\text{tot}}}$ and $\frac{\Gamma_\text{n}\Gamma_\text{p}}{\Gamma_{\text{tot}}}$ are given (one resonance)
5. $\frac{\Gamma_\text{n}\Gamma_\text{p}}{\Gamma_{\text{tot}}}$ is given (one resonance)

Uncertainty estimates are given in all these cases, and before completing the data, the widths that *are* reported are sampled for each random set of ND to be produced, as in Sec. III A 1.

Note that for all the 8 incompletely measured resonances, Γ_n, ℓ and J are missing. In case 1, we implicitly have Γ_n, but the $\Gamma_{\text{tot}}, \Gamma_\gamma, \Gamma_\alpha$ and Γ_p are sampled and Γ_n is computed by subtracting the partial widths from the total for each set of random ND.

First, ℓ and J are determined. It is assumed that $\ell \in \{0, 1\}$ for all levels. Within this restriction, the likelihood for each possible (ℓ, J) is computed, using the widths that are reported. This is done given the average level spacing and resonance widths as well as the distributions for the resonance energies and widths assumed in Sec. III A 2. Mathematically, we make use of Bayes' theorem with a constant prior, giving

$$P\left(\ell, J|\boldsymbol{\Gamma} = \boldsymbol{\gamma}, H = h\right) = \frac{f_{\boldsymbol{\Gamma}|(\ell,J)}(\boldsymbol{\gamma}) f_{H|(\ell,J)}(h)}{\sum_{(\ell',J')} f_{\boldsymbol{\Gamma}|(\ell',J')}(\boldsymbol{\gamma}) f_{H|(\ell',J')}(h)}, \tag{C1}$$

where

- $\boldsymbol{\Gamma}$ is the vector of the partial resonance widths that are reported (seen as a random vector).
- $\boldsymbol{\gamma}$ is the actual observation of $\boldsymbol{\Gamma}$ (the reported widths).
- H is the random variable describing the distance to the closest reported resonance with this (ℓ, J). The quantum numbers (ℓ, J) are determined in order of increasing energy, and H is affected by resonances with previously determined (ℓ, J). For resonances located in between completely reported resonances, the usage of the closest resonance to define H is a simplification; resonances on both sides will in reality affect the Wigner distribution below.
- h is the observation of H.
- $P\left(\ell, J|\boldsymbol{\Gamma} = \boldsymbol{\gamma}, H = h\right)$ is the probability of observing the quantum numbers (ℓ, J), given the reported widths $\boldsymbol{\gamma}$ and the distance to the closest resonance (with the considered (ℓ, J)) h (*i.e.*, what we want).
- $f_{\boldsymbol{\Gamma}|(\ell,J)}(\boldsymbol{\gamma})$ is the probability density for $\boldsymbol{\Gamma}$ given (ℓ, J), evaluated at $\boldsymbol{\gamma}$. The PDF is taken to be product of the PDFs of the individual partial widths, *i.e.*, the χ^2-distribution with DOFs as assumed in Sec. III A 2, and with expected values determined by the average partial widths given by TALYS for the particular random set of parameters for the (ℓ, J) under consideration.
- $f_{H|(\ell,J)}(h)$ is the probability density for H given (ℓ, J), evaluated at h. The PDF is based on the Wigner distribution using the average level spacing $D^{\ell,J}(E_\lambda)$ from TALYS. However, there is a risk that there is a closer resonance with the considered (ℓ, J) which is not observed, *i.e.*, that the observed resonance is an observation of the sum of two or more Wigner distributed variables. This is treated using the law of total probability, giving that

$$f_{H|(\ell,J)}(h) = \sum_{j=0}^{\infty} f_{H|(\ell,J),A_j}(h) P(A_j), \tag{C2}$$

where A_j is the event that j resonances are between this resonance and the closest reported resonance (all with the considered (ℓ, J)) and $P(A_j)$ is the probability for A_j. Assuming that the probability for a resonance to be missing is p, one gets $P(A_j) = (1-p)p^j$. For each random set of ND, p is set to

$$p = \frac{\langle n_\text{R}\rangle - n_{\text{R,H}}}{\langle n_\text{R}\rangle}, \tag{C3}$$

where $\langle n_\text{R}\rangle$ is the expected number of resonances in the range $0 < E \leq 17.2\,\text{keV}$ according to the average level spacings provided by TALYS (in this particular random run), and $n_{\text{R,H}} = 15$ is the number of resonances reported by Harvey in this range (many without reported (ℓ, J)). This gives p centered about 36 %.

Now, $H|A_j$ can be seen as the sum of $j+1$ independent Wigner distributed random variables. Because this is a rather small detail in the study, the coarse assumption that the central limit theorem can be applied for $j > 0$ is made. This gives that for $j > 0$, $f_{H|(\ell,J),A_j}(h)$ follows a normal distribution with expected value $(j+1)D^{\ell,J}(E_\lambda)$ and standard deviation $\sqrt{j+1}D^{\ell,J}(E_\lambda)/2$. At any point, the infinite series converges quickly due to the factor p^j. Thus,

$$f_{H|(\ell,J)}(h) \approx \frac{1-p}{1-p^K} f_{H|(\ell,J),A_0}(h) + \frac{1-p}{1-p^K} \sum_{j=1}^{K} p^j \varphi(h; (j+1)D^{\ell,J}(E_\lambda), \sqrt{j+1}D^{\ell,J}/2), \tag{C4}$$

where $\varphi(h; \mu, \sigma)$ denotes the PDF for the normal distribution with expected value μ and standard deviation σ. The upper summation limit K is chosen such that $p^K < 0.001$.

The resulting relative frequencies for the different possible (ℓ, J) are shown in Table VIII. The samples are

TABLE VIII: The observed relative frequencies of (ℓ, J) resulting from the sampling used when values are not provided by Harvey.

E_λ (Harvey)	$(0,1)$	$(0,2)$	$(1,0)$	$(1,1)$	$(1,2)$	$(1,3)$
6230.0	1.0(6)	55(3)	4(1)	23(2)	17(2)	0
6360.0	4(1)	39(3)	3(1)	25(2)	29(3)	0
9227.0	3(1)	26(3)	4(1)	3(1)	64(3)	0
9850.0	3(1)	33(3)	2.0(8)	10(2)	52(3)	0
11100.0	1.3(7)	44(3)	0	0	54(3)	0
11530.0	2.3(9)	47(3)	.3(3)	2.7(9)	48(3)	0
14400.0	22(2)	27(3)	3(1)	16(2)	31(3)	0
17200.0	10(2)	35(3)	2.7(9)	20(2)	32(3)	0

rather spread out, but with generally greater frequencies for $(\ell, J) = (0, 2)$ and $(\ell, J) = (1, 2)$, while $(\ell, J) = (1, 0)$ and there are no observations of $(\ell, J) = (1, 3)$. The two latter combinations are not reported by Harvey for any of the resonances, which can reduce $f_{H|(\ell,J)}(h)$. A substantially greater level spacing for $(\ell, J) = (1, 0)$ than for $(\ell, J) = (1, 3)$ can explain while the former occurs and not the latter.

With (ℓ, J) determined, the missing widths are determined using the reported information combined with the average widths from the random TALYS runs. The details differ between the 5 different cases described above. Case 1 is discussed earlier. For case 3, the missing widths are sampled directly from the random TALYS results as in Sec. III A 2. In case 2, the *proportion* of the missing widths is sampled from the TALYS results, but normalized such that that $\Gamma_{\text{tot}} = \Gamma_{\text{n}} + \Gamma_\gamma + \Gamma_\alpha + \Gamma_{\text{p}}$.

Cases 4 and 5 are a bit more complicated. For convenience, a and b are defined as

$$a = \frac{\Gamma_{\text{n}}\Gamma_\alpha}{\Gamma_{\text{tot}}}, \tag{C5}$$

and

$$b = \frac{\Gamma_{\text{n}}\Gamma_{\text{p}}}{\Gamma_{\text{tot}}}, \tag{C6}$$

respectively. In case 5, we can evaluate Γ_{tot} and rearrange the latter equation to obtain

$$\Gamma_{\text{p}} = \frac{b(\Gamma_{\text{n}} + \Gamma_\gamma + \Gamma_\alpha)}{\Gamma_{\text{n}} - b}. \tag{C7}$$

The widths $\Gamma_{\text{n}}, \Gamma_\gamma$ and Γ_α are then sampled as in Sec. III A 2 and b is sampled from the experimental information as in Sec. III A 1. Note, however, that $\Gamma_{\text{n}}\Gamma_{\text{tot}} > \Gamma_{\text{n}}\Gamma_{\text{p}}$ giving $\Gamma_{\text{n}} > b$. Therefore, the sampling is repeated until this condition is fulfilled, once again motivated by Eq. (B1). For most random sets, no repetition is necessary.

In case 4, Eq. (C5) can be divided by Eq. (C6) to yield

$$\Gamma_\alpha = \frac{a\Gamma_{\text{p}}}{b}. \tag{C8}$$

Inserting this into Eq. (C7) gives

$$\Gamma_{\text{p}} = \frac{b(\Gamma_{\text{n}} + \Gamma_\gamma)}{\Gamma_{\text{n}} - a - b}. \tag{C9}$$

This time, only Γ_{n} and Γ_γ are sampled as in Sec. III A 2 while a and b are sampled from the experimental information. Γ_{p} is then back-substituted into Eq. (C8) to yield Γ_α. In this case, the sampling is repeated (if necessary) until $\Gamma_{\text{n}} > a + b$ since this condition is implied by $\Gamma_{\text{n}}\Gamma_{\text{tot}} > \Gamma_{\text{n}}(\Gamma_\alpha + \Gamma_{\text{p}})$.

[1] C. Nordling, J. Österman, Physics Handbook, 8th Edition, Studentlitteratur, 2006.
[2] S. Mughabghab, Atlas of Neutron Resonances, Elsevier Science, 2006.
[3] F. Garner, Radiation damage in austenitic steels, Comprehensive Nuclear Materials 4, 33 (2012).
[4] M. Chadwick, et al., ENDF/B-VII.1, Nuclear data for science and technology: Cross sections, covariances, fission product yields and decay data, Nuclear Data Sheets 112, 2887 (2011).
[5] A. Koning, et al., The JEFF-3.1 nuclear data library, JEFF report 21, Tech. rep., OECD-NEA (2006).
[6] H. Gruppelaar, et al., Evaluation of neutron cross sections and photon-production data for Ni-isotopes in the energy range 0-20 MeV, Tech. rep., ECN (1990).
[7] A. Koning, D. Rochman, Towards sustainable nuclear energy: Putting nuclear physics to work, Annals of Nuclear Energy 35, 2024 (2008).
[8] A. Koning, D. Rochman, Modern nuclear data evaluation with the TALYS code system, Nuclear Data Sheets 113, 2841 (2012).
[9] A. Trkov, M. Herman, D. Brown, et al., ENDF-6 formats manual, Tech. Rep. BNL-990365-2009, Brookhaven National Laboratory (2011).
[10] N. Otuka, et al., Towards a more complete and accurate experimental nuclear reaction data library (EXFOR): International collaboration between nuclear reaction data centres (NRDC), Nuclear Data Sheets 120, 272 (2014).
[11] P. Helgesson, H. Sjöstrand, A. Koning, J. Rydén, D. Rochman, E. Alhassan, S. Pomp, Sampling of systematic errors to estimate likelihood weights in nuclear data uncertainty propagation, Nuclear Instruments and Methods in Physics Research A 807, 137 (2016).
[12] R. Werner, D. Santry, Measured thermal-neutron cross section for the ^{59}Ni(n,α)^{56}Fe reaction, Nuclear Science and Engineering 56 , 98 (1) (1975).
[13] H. Eiland, G. Kirouac, Measurements of the ^{59}Ni(n,α) cross section for thermal neutrons, Nuclear Science and Engineering 53, 1 (1974).
[14] P. Schillebeeckx, et al., Determination of resonance parameters and their covariances from neutron induced reaction cross section data, Nuclear Data Sheets 113, 3054 (2012).
[15] J. McDonald, N. Sjöstrand, Measurements of thermal

neutron cross sections for helium production in ^{59}Ni, Nuclear Cross Sections and Technology 2, 810 (1975).
[16] M. Ashgar, A. Emsallem, N. Sjöstrand, Thermal neutron induced charged particle reactions on ^{58,59,61}Ni, Zeitschrift für Physik A 282, 375 (1977).
[17] S. Raman, et al., Thermal neutron capture by ^{58}Ni, ^{59}Ni and ^{60}Ni, Physical Review C 70. doi:044318.
[18] A. Carlson, et al., International evaluation of neutron cross section standards, Nuclear Data Sheets 110, 3215 (2009).
[19] D. Neudecker, R. Frühwirth, H. Leeb, Peelle's Pertinent Puzzle: A fake due to improper analysis, Nuclear Science and Engineering 170, 54 (2011).
[20] R. Peelle, Peelle's Pertinent Puzzle, Informal ORNL memorandum (1987).
[21] G. D'Agostini, On the use of the covariance matrix to fit correlated data, Nuclear Instruments and Methods A 346, 306 (1994).
[22] D. Smith, Probability, Statistics, and Data Uncertainties in Nuclear Science and Technology, American Nuclear Society, LaGrange Park, IL, USA, 1991.
[23] P. Helgesson, D. Rochman, H. Sjöstrand, E. Alhassan, A. Koning, UO_2 vs MOX: Propagated nuclear data uncertainty for k_{eff}, with burnup, Nuclear Science and Engineering 177, 321 (3) (2014).
[24] A. Koning, et al., TALYS-1.8, User Manual, Nuclear Research and Consultancy Group NRG (December 2015).
[25] R. MacFarlane, A. Kahler, Methods for processing ENDF/B-VII with NJOY, Nuclear Data Sheets 111, 2739 (2010).
[26] D. Rochman, A. Koning, J. Kopecky, J.-C. Sublet, P. Ribon, M. Moxon, From average parameters to statistical resolved resonances, Annals of Nuclear Energy 51, 60 (2013).
[27] D. Rochman, S. Goriely, A. Koning, H. Ferroukhi, Radiative neutron capture: Hauser Fesbach vs. statistical resonances, Physics Letters B 764, 109 (2017).
[28] Python language reference, version 2.7.13, Python Software Foundation, Available at www.python.org, June 30, 2017.
[29] T. Oliphant, Python for scientific computing, Computing in Science and Engineering 9, 10 (2007).
[30] A. Koning, Bayesian Monte Carlo for nuclear data evaluation, European Physics Journal A 51, 184 (2015).
[31] A. Afifi, S. Azen, Statistical analysis, A computer oriented approach, 2nd Edition, Academic Press, New York, NY, USA, 1979.
[32] P. Stelson, ORNL physics division annual progress report for period ending December 31, 1975, Tech. Rep. ORNL-5137, Oak Ridge National Lab (May 1976).
[33] D. Pelowitz, et al., MCNP6 User's Manual 2.7.0, Los Alamos National Lab. (December 2012).
[34] M. Pescarini, V. Sinitsa, R. Orsi, M. Frisoni, ENEA-Bologna multi-group cross section libraries for LWR shielding and pressure vessel dosimetry applications, Tech. Rep. RdS/2011/122, ENEA (2011).
[35] D. Rochman, W. Zwermann, S. van der Marck, A. Koning, H. Sjöstrand, P. Helgesson, B. Krzykacz-Hausmann, Efficient use of Monte Carlo: Uncertainty propagation, Nuclear Science and Engineering 177, 337 (2014).
[36] G. Casella, R. Berger, Statistical Inference, 2nd Edition, Thomson Learning, Pacific Grove, CA, USA, 2001.
[37] G. Kirouac, Calculated thermal (n,α) cross section for Ni-59, Nuclear Science and Engineering 46, 427 (1971).
[38] A. Gut, An Intermediate Course in Probability, Springer-Verlag, New York, 1995.